A New Approach to Study the Degradation of the Organic Pollutants by A-Doped MxOy/B Photocatalysts

Mojtaba Arabameri
University of Kashan
Hadis Bashiri (h.bashiri@ymail.com)
University of Kashan https://orcid.org/0000-0002-1049-7984

Research Article

Keywords: Photodegradation, Organic pollutants, Comprehensive mechanism, Reactive-centers, Effective charge carriers, Hybrid manual-automatic method

Posted Date: September 27th, 2021

DOI: https://doi.org/10.21203/rs.3.rs-885999/v1

A New Approach to Study the Degradation of the Organic Pollutants by A-doped M_xO_y/B Photocatalysts

*Mojtaba Arabameri and Hadis Bashiri**

Department of Physical Chemistry, Faculty of Chemistry, University of Kashan, Kashan, Iran

*To correspondence should be addressed. Fax: +98 31 55912397.

Email: hbashiri@kashanu.ac.ir and h.bashiri@ymail.com

Abstract

This work presents a new approach and a comprehensive mechanism to study the kinetics of the photodegradation of the organic pollutants. The vital role of various operational factors on the degradation of the organic pollutants is explained using this method. The proposed approach is based on the simple strategies and a powerful computational method. Two new variables "the effective concentration of photon" (I_{eff}) and "the effective concentration of the reactive-centers" (RC) are defined to better understanding the effect of operational parameters on the organic pollutants photodegradation. The optimum conditions of the photocatalytic degradation can be determined with the help of this method. This approach was used to study the kinetics of photodegradation of the organic pollutants on the $\mathrm{A-doped\,M_xO_y/B}$ photocatalysts. The provided mechanism has been examined with the some experimental data. The high correlations between the experimental data and the fitting results under different conditions prove this mechanism could be reliable.

Keywords: Photodegradation; Organic pollutants; Comprehensive mechanism; Reactive-centers; Effective charge carriers; Hybrid manual-automatic method.

1. Introduction

Water is one of the essential needs of all life-supporting processes (Westall &Brack 2018). One of the most important challenges of today's society is providing safe drinking water for all people (Khalifa &Bidaisee 2018, Reina et al. 2015). The water sources are at severe risk of pollution due to the growth of the various pollutant activities such as industrial waste effluents, agricultural runoff, pharmaceuticals disposal, urban sewage draining, and landfill seepage (Hu et al. 2013, Malakootian et al. 2019). Some authors have believed that textile industry wastewater is the most polluting among the various industrial fields (Liang et al. 2014, Verma et al. 2012). Waste effluents of the textile industry usually contain a high concentration of pigments, dyes, and toxic materials (Lau &Ismail 2009). It has been reported that synthetic dyes are among the major pollutants of water because of their toxic and carcinogenic characteristics (Lai et al. 2014).

The results of various researches show that advanced oxidation processes (AOPs) are suitable techniques for removing toxic materials (Ghatak 2014, Navarro et al. 2017, Samadi et al. 2017, Stets et al. 2018, Zhou et al. 2019). This technique is based on the *in situ* production of strong oxidizing intermediates such as superoxide radical anions ($O_2^{\bullet -}$), hydroxyl radicals ($OH^{\bullet}$), hydrogen peroxide (H_2O_2), and singlet oxygen ($^1O_2$). AOPs include the different types of processes such as the chemical (Fe^{2+}/H_2O_2, O_3 /H_2O_2), the photochemical (UV/H_2O_2, UV/O_3, $UV/Fe^{2+}/H_2O_2$, UV/TiO_2), the son-chemical (UV/H_2O_2, UV/O_3) and the electrochemical technologies (Al-Kdasi et al. 2004, Vagı &Petsas 2017).

Heterogeneous photocatalysis is an advanced technology to deal with environmental pollution (Al-Rasheed 2005, Ibhadon &Fitzpatrick 2013, Liu et al. 2014, Simon et al. 2020). It can be defined as 'the acceleration of a chemical reaction by using a photocatalyst under light's irradiation with adequate energy.' In recent years, many semiconductor metal oxides such as TiO_2 (Gupta et al. 2012), ZnO (Chakrabarti &Dutta 2004), Fe_2O_3 (Hitam &Jalil 2020), NiO

(Sabouri et al. 2018), CdS (Khan et al. 2016), and WO_3 (Yao et al. 2017) have been widely studied for the decomposition of the organic contaminants under visible light and UV irradiation. Titanium dioxide and zinc oxide have received much attention in the field of pollutants photodegradation research. These photocatalysts are non-toxic, low-cost, highly efficient, and environmentally friendly (Xia et al. 2016).

In general, a photocatalytic process involves the following steps: (1) photon absorption with energy equal to or greater than the bandgap of the semiconductor, (2) the electron transfer from the valence band (VB) to the conduction band (CB) for the producing electron-hole pairs, (3) the trapping of the charge carriers on the effective reactive-centers during light illumination, and (4) the degradation of toxic compounds by the powerful oxidizing agents:

$$\mathrm{A-doped\ M_xO_y/B} + h\nu \rightarrow e^- + h^+ \quad (1)$$

$$e^- + h^+ + \text{The effective reactive} - \text{centers} \rightarrow \text{The powerful oxidizing agents} \quad (2)$$

$$\text{The powerful oxidizing agents} + \text{Pollutant} \rightarrow \text{Intermediates} \quad (3)$$

Although the kinetics of photocatalytic reactions have been extensively investigated, more work is needed to gain the sufficient knowledge about the mechanism of these reactions. Many researchers have investigated the mechanism of photocatalytic reactions based on experiment results, identification of the reactive oxygen species, and studying the behavior of the reaction intermediates (Berberidou et al. 2016, Dror et al. 2020, El Mragui et al. 2019, Kaur &Sud 2012).

To the best of our knowledge, some articles have discussed the mechanism of the photocatalytic reactions, and they have proposed the general mechanisms or the possible pathways for photocatalytic reactions (Huang et al. 2020, Turkten &Cinar 2017, Wang et al. 2018). Some articles have studied the kinetics of the photocatalytic process based on a proposed mechanism (Emeline et al. 2000, Minero et al. 2013, Montoya et al. 2014). Unfortunately, the detailed mechanism at the atomic scale has been introduced for a limited number of

photocatalysts (Nosaka &Nosaka 2017). However, only few articles describe the photodegradation mechanism involving the elementary steps of the reaction and their rate constant values (Bashiri et al. 2014, Bashiri &Pourbeiram 2016, Shams Ghamsari &Bashiri 2020).

In this paper, a new approach was proposed to study the kinetics and mechanism of the degradation of the organic pollutants by the various photocatalysts under UV-Vis light illumination. Without the use of common kinetic approximations, this approach helped us to gain a better understanding of the various steps of photocatalytic processes, such as the electron-hole generation step. The surface of semiconductors is a crucial factor for many applications such as pollutants photodegradation, solar cells, and microelectronic systems. A detailed understanding of their surface structure is essential for developing the mechanism of the pollutants photodegradation.

Our approach assumes the photodegradation of organic compounds occurs due to the effective charge carriers and the formation of the effective reactive-centers on the $\mathrm{A-doped\ M_xO_y/B}$ surface. Therefore, the two variables named the effective concentration of photon (I_{eff}) and effective concentration of the reactive-centers (RC) are defined for a better understanding the effect of operational parameters on pollutants photodegradation. Because a small number of the reactive-centers and the charge carriers lead to the degradation of organic pollutant. Interestingly, these variables reach the maximum or minimum when the system is in optimal condition.

The $\mathrm{A-doped\ M_xO_y/B}$ general formula was proposed to demonstrate the flexibility of our method. The $\mathrm{M_xO_y}$ is a semiconductor, such as TiO_2 and ZnO, which can interact with water species, oxygen molecules, and other materials to form the various reactive-centers. A is a metallic or non-metallic element that can increase the photocatalytic activity of the $\mathrm{M_xO_y}$ photocatalyst.

The interaction of water species and the pollutant molecules with the $A-\text{doped } M_xO_y/B$ surface is an critical step in the degradation mechanism (Thiel &Madey 1987, Vittadini et al. 2007). The adsorbed water species on the surface of photocatalysts are oxidized by the valence band holes to produce the hydroxyl radicals (Muhd Julkapli et al. 2014). These processes leads to the production of the reactive-centers for the degradation of organic pollutant molecules.

The B component can be a compound such as graphic carbon nitride, reduced graphene oxide, ozone, montmorillonite, another photocatalyst, or even a mixture of them. The interaction of B component with some species in the system, such as oxygen molecules and water species, leads to the formation of the other reactive-centers. The coupling these materials with a photocatalyst can be a suitable method to achieve enhanced photocatalytic activity.

In the present investigation, MATLAB software was used as a computational tool to solve the differential rate equations by a deterministic method. Four sets of experimental data from some literature were used to examine this approach. These systems are listed in Table 1. The vital role of various operational parameters in the photodegradation of pollutants was easily explained using this approach. The values of rate constants for elementary reactions and the effective concentrations of the reactive-centers were obtained by combining manual and automated methods. The conformity between the experimental data and fitting results was examined under different operating conditions.

The production of the electron-hole pairs, dye adsorption on the photocatalyst surface, the trapping of the charge carriers to produce the reactive radicals, and the recombination of the charge carriers have the key effects on the photodegradation of the organic pollutants. In this study, a proposed approach has been used to theoretically investigate the effects of these factors on the degradation process of the organic pollutants without using the common kinetics approximations. Therefore, a non-approximation approach is proposed to study the kinetics and mechanism of the photocatalytic reactions. Obviously, a complex kinetics equation can be

obtained using the proposed mechanism and the kinetics approximations such as the steady-state approximation. This complex kinetics equation can be reduced to a Langmuir-Hinshelwood equation by considering more approximations. It is not possible to solve this equation analytically by standard methods. However, a concise mechanism and multiple approximations must be used to derive a simple kinetics equation such as the first-order equation.

The real mechanism of the photodegradation of organic pollutants involves several steps, and their nature is not fully understood. These kind of processes depend on various experimental conditions including the type of reactants, the solution pH, the concentration of reactants, and the photocatalyst surface structure. A suitable method for studying the mechanism of the photocatalytic reactions is to estimate the rate constants and to investigate the effect of different factors on their values. A detailed understanding of the photodegradation process of the organic pollutants by photocatalysis helps us to properly design a photocatalytic experiment. However, this approach provides more information about the generation process of the electron-hole pairs. On the one hand, the importance of our work is that it proposes the rate constants of a photocatalytic process without any approximation. The different samples can be compared in a photocatalytic system by using the rate constants of this step and the effective variables. In addition, a useful comparison between the rate constants of the first step and the rate constants of the other steps is provided by a proposed variable named as “the effective concentration of photons”.

2. Methods: the estimation of the rate constants and the effective variables

The mechanism of a chemical reaction consists of a series of elementary chemical reactions. Usually, the rate constants and initial concentration of the sites are identified using the

parameters estimation procedures. Mathematical methods for studying the kinetics and mechanisms of chemical reactions can be stochastic or deterministic.

The stochastic method regards the time evolution of the chemical reaction as a random-walk process that is described by a differential equation (the chemical master equation) (Bashiri &Mohamadi 2016, Bashiri &Pourbeiram 2016, Rafiee &Bashiri 2019, 2020b, a, Shams Ghamsari &Bashiri 2020). The deterministic method regards time evolution of the chemical system as a continuous process that can be governed by a series of coupled ordinary differential equations (ODEs). In our work, the deterministic method was used to solve a series of rate equations that describe the photocatalytic process. The fitting data of the organic pollutants concentration versus time are obtained by integration of the ODEs. For the implementation of the deterministic method, the numerical techniques can be used to solve the differential rate equations. The results of various researches showed that the performance of stochastic and deterministic methods strongly depends on the studied system (Lerkkasemsan 2010, Safieddine et al. 2012, Zheng &Ross 1991).

We used MATLAB code framework based on the following parts: (1) experimental data, initial concentrations, and initial guesses of rate constants are the inputs, (2) the rate equations of the elementary steps are written, (3) odes15s solver is used (4) the commands for the drawing curves are used, (5) the codes related to the minimization are applied.

MATLAB software uses various solvers such as ode23, ode45, ode15s, ode23s, and ode113 to solve the ODEs. Ordinary differential equations can be classified as stiff and non-stiff. Shampine et al. (Shampine &Reichelt 1997) believed that this classification plays a crucial role in selecting the solvers. Stiffness is an essential and efficient concept in the numerical integration of the ODEs. It is generally accepted that a differential equation is stiff if the explicit numerical methods do not provide the appropriate solutions to the given equation. The stiffness phenomenon depends on the initial conditions, the ordinary differential equations,

and the numerical algorithm. Some algorithms are defined for non-stiff equations and some others for stiff equations.

MATLAB documentation suggests the ode45 is the best solver for solving problems in the first step. Many problems have been solved by the ode45 solver, which is based on a Runge-Kutta method (Forsythe 1977). The next suggestion is that the ode15s solver can be used if the ode45 fails or is extremely slow. In this work, the integration of the ODEs was performed by using the ode15s solver from MATLAB version, R2015b. The ode15s is a variable-order and multi-step solver that is used to solve stiff differential equations. The ode15s algorithm is based on the implementing of the backward differences of a set of numerical differentiation formulas (NDFs) (Shampine &Reichelt 1997).

Several numerical methods such as Euler, Runge–Kutta, Adams–Bashforth, and Adams–Moulton are used for solving the system of differential equations. These methods are divided into two categories single-step and multi-step methods. The Backward difference formula (BDF) is a general method for solving stiff differential equations. The BDFs are a set of implicit methods for the numerically solving of the differential equations. A system of differential equations can be written as follows:

$$F\big(t.x(t).x'(t)\big) = 0; x(t_0) = x_0 \tag{4}$$

The simplest BDF method is the Backward Euler method, which involves replacing the x derivative by a backward difference:

$$F\left(t_{\mathrm{n}}, x_{\mathrm{n}}, \frac{x_{\mathrm{n}} - x_{\mathrm{n-1}}}{h}\right) = 0;\ h = t_{\mathrm{n}} - t_{\mathrm{n-1}} \tag{5}$$

Where *h* is the step size. MATLAB implements an ode15s solver based on the BDF method. Therefore, MATLAB solves the ODEs using the ode15s algorithm in this work. Then, the results were compared with experimental data. If there was no good fit, the input values were readjusted to obtain a coefficient of determination close to 1.

Generally, the rate constants for each step and the effective variables are the adjustable parameters obtained through the fitting process in the MATLAB environment. In this study, two methods of parameter estimation are employed to examine the final mechanism: the hybrid manual-automatic method and the optimization technique. The first method is the estimation of parameters in two steps: (1) the rate constants and initial concentrations of the reactive-centers are manually adjusted to obtain a coefficient of determination close to 1; (2) the minimization function of the '$fminsearch$' is used to optimize the rate constants. In the second method, the rate constants are estimated in one step using the '$fmincon$' minimization function. The $fminsearch$ function minimizes an unconstrained multivariable function by using the Nelder– Mead simplex method. This method is a direct algorithm, which is used to minimize the nonlinear functions. The '$fmincon$' function is an iterative method that starts from an initial point and converges to a constrained local minimum. In our simulations, the '$fmincon$' function implements the 'interior-point' algorithm at each iteration using second-order gradient methods. The interior-point algorithm solves a sequence of unconstrained minimization problems to approach the constrained optimization.

In this work, the sum of squared errors (SSE) between the fitted and experimental data is used as an objective function of the optimization process.

$$\text{Objective function} = \text{SSE} = \sum (x_{\text{pred}}(i) - x_{\text{exp}}(i))^2 \quad (6)$$

Where, the variables x_{pred} and x_{exp} are the predicted and experimental data of x, respectively. In each run, the program calculates the coefficient of determination (R-square) using the mean-square error for easy comparison of the results. The coefficient of determination of the collection of the (t, C) points can be defined as:

$$R^2 = 1 - \left(\frac{\text{SSE}}{\text{SST}}\right) \quad (7)$$

Where, SST is the total sum of squares (variance), which is obtained as follows:

$$\mathrm{SST} = \sum (x_{\exp}(i) - \bar{x}(i))^2 \quad (8)$$

Where, $\bar{x}$ is the mean of the experimental data.

3. Results and Discussion

3.1. Basics of the proposed approach

The photodegradation process of the pollutant depends on several intrinsic and extrinsic factors. The photocatalyst properties such as surface area, crystallinity, morphology, and the doping of other elements into its lattice refer to the intrinsic factors (Friedmann et al. 2010). The other factors such as irradiation light source, the concentration of organic pollutants, catalyst loading, reaction temperature, pH value, and the presence of dissolved substances are related to extrinsic factors (Wan et al. 2014).

The interaction of the catalyst with other substances in the solution under UV/vis light illumination leads us to define a set of the reactive-centers on the photocatalyst surface. The basic assumption of our approach is that photodegradation process is controlled by the effective reactive-centers on the surface of the photocatalyst. The formula of the reactive-centers is shown in Table 2.

In addition, the proposed approach is based on several other strategies as follows: (1) effective concentration of photon and the effective concentration of the reactive-centers can be considered as an efficiency criterion of the photocatalytic process, (2) the trapping the photogenerated electrons and holes plays a vital role in the degradation of organic pollutants, (3) the adsorption of dissolved species on the catalyst surface is one of the crucial factors in the photocatalytic activity, (4) surface-adsorbed radicals ($OH^{\bullet}(ads)$ and $O_2^{-\bullet}(ads)$) are main reactive species formed in the photodegradation process, (5) the doping of the other elements into the photocatalyst lattices can significantly promote the destruction of the organic pollutants molecules, (6) the inactivation parameters in the photocatalytic system have a critical impact

on the performance of the degradation reaction, (7) intermediates have a crucial effect on the rate of organic pollutants degradation due to the simultaneous reaction with reactive oxygen species formed in the solution.

As shown in Figure 1, our approach to the photodegradation of organic pollutants involves the following steps: (1) a certain number of the reactive-centers are defined on the surface of the TiO_2, (2) based on the proposed model, the reaction pathway is decomposed into a series of elementary reactions, (3) a suitable software with high computing power (MATLAB) is selected, (4) an initial value is suggested for each the rate constant, and the effective concentration of the reactive-centers, (5) the required codes were written in MATLAB environment to run the data fitting process, (6) the data fitting program was performed to examine the reaction mechanism, (7) the fitted and experimental data were compared by plotting the pollutant concentration versus time and computing the R^2, (8) if the fitting is not right, the kinetics factors (elementary steps and the rate constants) or the effective concentration of reactive-centers will be changed, (9) the fitting process is terminated when the best fitting is obtained. In other words, an initial mechanism is constructed based on the proposed approach. The fitting codes are written in a MATLAB computing environment.

The reliable fitting results are obtained by adjusting the rate constants of the elementary steps and the concentrations of the reactive-centers. If a good fit is not found, another mechanism should be proposed. The initial guess for the rate constants is generated using the literature's values (Bashiri et al. 2014) or our suggested values.

However, it is impossible to propose a unique and comprehensive mechanism for photocatalytic reactions due to the various factors and their influence on the degradation process. Therefore, to obtain the best conformity between the experimental and the simulated data, it is necessary to examine the different mechanisms of pollutant degradation.

3.2. The mechanism of the pollutant photodegradation

In general, three categories of mechanisms have been proposed for the degradation of organic pollutants by photocatalysts under UV-Vis light.

In the first category of mechanisms, the hydroxyl radicals are the main oxidant of the pollutant's degradation. Achieving this mechanism requires the production of powerful holes. These holes are produced by the action of the UV-light on the surface of a photocatalyst with the suitable bandgap. The systems of the TiO_2/UV, Ni-doped ZnO/UV, and Fe-doped TiO_2/UV are considered in this category.

In the second category of mechanisms, the superoxide radicals are the main oxidant of the pollutant degradation. In these systems, there are not powerful photogenerated holes to oxidize the water species. The systems of the TiO_2/Vis-light, N-TiO_2/Vis-light, and N-TiO_2/RGO/Vis-light are in the second category of the mechanisms.

For non-doping TiO_2 under visible light irradiation, it has been suggested (Liu et al. 2000) that an adsorbed pollutant molecule is excited to the singlet or triplet states; subsequently an electron is injected from the excited pollutant molecule to the TiO_2 conduction band to produce a pollutant cationic radical (pollutant$^{\bullet+}$). This excited molecule undergoes the degradation process to produce the intermediates. The visible-light-induced electrons react with O_2 molecules and produce the superoxide radicals. This mechanism is also called the photosensitized oxidation mechanism.

When N-doped TiO_2 or N-doped TiO_2/RGO are exposed by the visible light irradiation, the photogenerated electrons are transferred from the localized N levels in the TiO_2 band gap (the mid-gap states) to the conduction band. These electrons in the conduction band are trapped by the O_2 pre-adsorbed on the TiO_2 surface or the RGO surface to produce the superoxide radicals.

The electron spin resonance (ESR) experiments using the spin-trap, 5,5-dimethylpyrroline-1-oxide (DMPO), showed (Rengifo-Herrera et al. 2009) the oxidative potential of the photoinduced holes associated with the mid-gap states have not high power to produce the hydroxyl radicals (2.38 V (SHE)). Some researchers ignore this argument and consider the reaction of water species to visible light-induced holes (Chen &Liu 2016). For the systems of the N-doped TiO_2 and N-doped TiO_2/RGO, the reaction of the visible-light-induced holes with water species was neglected in our method. However, the reaction of the holes with the adsorbed pollutant molecules on the photocatalyst surface is considered.

In the third category of mechanisms, the free photogenerated holes are the main factor of degradation of organic pollutants. In some systems that follow the first type mechanism, adding new material to the photocatalyst structure may change the main oxidant. For example, the presence of the ozone in the Ag-doped ZnO/UV photocatalyst plays this role.

The general proposed framework for the mechanism of the degradation process of the organic pollutants in $(\mathrm{A-doped\ M_xO_y/B/UV-Vis})$ aqueous systems is shown in Table 3. In the present study, several mechanisms were examined, and among them, the final mechanism presented in Table 4 had the best agreement with the experimental data. Three general conclusions can be deduced from the final mechanism: (1) a general framework can be proposed for the degradation process of organic pollutant by the photocatalysts; (2) the rate constants of the elementary reactions in different systems have similar values; (3) the excellent conformity in the fitting process indicates that the proposed approach can be verified using the experimental data (Han et al. 2018, Mousavi et al. 2017, Peng et al. 2019, Tang et al. 2018) under different conditions.

Two methods of the optimization and manual adjustment were implemented simultaneously for the TiO_2/visible light/TC system to compare the correlation results (Figure 2). The correlation analysis on the fitting results shows that there is not much difference

between the R^2 values in the optimization and the manual adjustment methods. For this system, the elementary reaction steps and their rate constants are presented in Table 5. Perfect conformity between the adjusted and optimized values was found in this Table. This result shows that the MATLAB optimization method can be used well for simple systems.

However, the fitting results show that manual adjustment of the parameters leads to reliable values than the optimization-based procedure for the complicated systems. The main reasons can be explained as follows: (1) the number of parameters estimated in each run is large, (2) many operational factors are considered for the selecting of an appropriate mechanism, (3) the detailed mechanism of photocatalytic reactions involves many elementary steps. For this reason, we proposed a hybrid manual-automatic method.

3.2.1. The analysis of the curve of pollutant concentration versus time and the effect of the intermediates on the degradation process

The analysis of the plot of the concentration versus time is slightly complicated. The shape of this curve qualitatively reflects the behavior of the photocatalytic system. In general, the curves of pollutant concentration versus time can be divided into three steps. In the first step, the ROSs mainly react with the organic pollutant molecules. The fitting investigations show that in the initial times, the curve of organic pollutant concentration versus time is mainly affected by the interaction between the pollutant and ROSs. In other words, regardless of the intermediates reaction with the $OH^{\bullet}$ radicals, only the initial parts of the fitting curve have good conformity to the experimental points. The reaction of ROSs with the initial intermediates, which is produced in the photocatalytic process, is considered as the second step. The effect of other intermediates are taken into account in the third step.

From this view, the two types of mechanisms can be defined: degradation mechanism without and with the reactions of intermediates. The first type is only suitable to describe the

concentration vs. time at the initial times. The other type shows more agreement between the experimental and the fitting results after passing the time. In other words, a set of consecutive reactions occurs in which the produced intermediates are oxidized by the ROSs. The number of these reactions in the real system is large, but one or two reactions can be appropriate to obtain a good agreement. The rate constant of these consecutive reactions depend on the conditions of the studied system. After passing the time, the interaction between the intermediates of the degradation of organic pollutants and ROSs is also influential.

However, the steps of the hybrid manual-automatic adjusting of the system parameters and the concentrations of reactive centers can be explained as follows: (1) Based on the experimental results, the percentage of the ROSs participation in the pollutant degradation is approximately adjusted. The fitting process starts without considering the intermediates reactions. The values of the effective variables should be adjusted, and the fitting results should be as close as possible to the first experimental data. (2) the reaction of the first intermediate with the ROSs is considered, and the program is executed. The rate constant of this step is adjusted to obtain good conformity between the model predictions and the other experimental points. (3) the reactions of one or more intermediates with the ROSs are considered to obtain the excellent fitting results. (4) finally, the values of the rate constants are optimized by using the $fminsearch$ function.

The fitting results show the first intermediate competes significantly with the organic pollutant molecule to consume the hydroxyl radicals. These reactions are symbolically represented in the fifth part of the general mechanism. The rate constant of the consecutive steps is a function of the operational parameters and varies from 10^6 to 10^9 in the different conditions. The following reason can be used to explain this behavior. The ROSs reaction with pollutants may lead to the production of two types of intermediates. Since each of the

intermediates tends to react with the ROSs, the rate constant for these reactions varies slightly for the samples under study.

In this paper, four systems have been considered to examine the comprehensive mechanism of the degradation of the organic pollutant on the surface of the photocatalysts under different conditions. Figures 3 and 4 represent the fitting results for the studied samples. Figure 3 shows the trend of changes in the effective concentration of photon and the effective concentration of reactive-centers based on the proposed approach. In an overview, Figures 3 and 4 show that there are significant correlations between degradation efficiencies and the different parameters. In this paper, The effect of some operational parameters on the degradation efficiency will be discussed using these figures.

3.2.2. The production step of the photogenerated charge carriers

The first part of the proposed framework is the production of the charge carriers. Similar to other photocatalytic reactions (Galindo et al. 2000, Rauf et al. 2011), the proposed mechanism is initiated by photoexcitation of the photocatalyst or the pollutant under the UV-Vis light illumination. This step is very fast with a timescale in the order of 10^{-14} s (Dou et al. 2004, Friedmann et al. 2010). Nevertheless, our results showed the rate constant for the photoexcitation by the UV-light is in the order of 10^{-3} $M^{-1}.min^{-1}$, while the rate constant of the photoexcitation by visible light is in the order of 10^{-1} $M^{-1}.min^{-1}$. One reason for this difference may be that UV beams are more powerful than visible light. However, it seems that there is a mismatch between the timescale of charge carriers generation and the relatively low efficiency of photocatalytic reactions (Qian et al. 2019). This conclusion is an interesting result, because the fitting results show a significant difference between the physical and chemical understanding of the electron-hole generation process. In other words, the pollutant

photodegradation can result from a balance between the processes of adsorption, recombination, trapping, and interfacial transfer of the charge carriers.

As a result, the generation of effective electrons and holes is the first step in the proposed mechanism. For this reason, the rate constant of the production of the effective charge carriers may be reduced. Based on these arguments, the proposed approach assumes that a significant fraction of the incident light beams is scattered into the reaction vessel and does not lead to the generation of electrons and holes. Therefore, a minor fraction of the photogenerated carriers leads to degradation of the organic pollutant due to performance-limiting factors such as the recombination process and the photoreactor geometry. In other words, small number of electron-hole pairs generated by the intensity of the absorbed light contribute to the destruction of organic pollutant, and many of them are ineffective. This discussion proposes two variables, which are named as the effective concentration of photon (I_{eff}), and the effective concentration of reactive-centers (RC).

These variables depend on the system operational parameters, such as the initial pollutant concentration, photocatalyst loading, light intensity, the solution pH, and the volume of the reaction vessel. The effective concentration of photon refers to the effect of the charge carriers in the pollutant degradation. Besides, the effective concentration of reactive-centers indicates the role of the photocatalyst and its interaction with the other dissolved species in the degradation process. In our approach, the effective reactive-centers refer to the sites that play a direct role in the destruction of the organic pollutant. The structure and effective concentration of the reactive-centers depend on the following factors: (1) the structure of the photocatalyst; (2) the pH of the solution; (3) the species dissolved in the solution.

The pH of the solution is a critical parameter in the degradation of the pollutants under UV/visible irradiation. Because the medium pH determines the charges on the catalyst surface and the organic pollutant molecules. It is affected by various factors such as the charge values

on the semiconductor surface and organic pollutant molecules, ROSs concentration formed during the destruction process, and the aggregates' size. The influence of pH on the photocatalytic activity of the organic pollutant molecules has been investigated by several researchers (Alkaim et al. 2014, Kazeminezhad &Sadollahkhani 2016). Therefore, the structure of the reactive-centers depends on the solution's pH. In some cases, the degradation rate of the cationic organic pollutants in an acidic medium is greater than that of an alkaline solution (Devi et al. 2017). In the proposed method, this behavior is ascribed to the increase in the concentration of the hydroxyl groups originated from the interaction of the protons (or water molecules) with the surface oxygen sites.

For the $A-\text{doped}\,M_xO_y/B$ photocatalyst, the concentration of reactive-centers of $M-OH_2^+$, $M-O_{bridge}H-M$, $A-OH_2^+$, and $A-O_{bridge}H-A$ increases in the acidic pH due to the availability of sufficient protons. Also, the concentration of the $M-OH$, $M-O^-$, $A-OH$, and $A-O^-$ reactive-center increases at alkaline conditions. In a neutral medium, the reactive-centers produced by the interaction between non-dissociated water molecules and the M_xO_y surface are responsible for the degradation of the organic pollutant. It is worth noting that if A was not a metallic element, there is no effective interaction between this component and water species. The effective variables, especially I_{eff}, can be used to determine optimal operating conditions. During the fitting process, the rate constants, I_{eff} values, and the effective concentration of reactive-centers are adjusted simultaneously to obtain the best fitting between the experimental data and simulated results. Two significant results are obtained by the plotting of I_{eff} data against the values of operational parameters: (1) the optimum degradation conditions and (2) the effect of each parameter on the production process of the charge carriers.

3.2.3. The adsorption of the pollutant on the photocatalyst surface

The second part of the proposed mechanism refers to the adsorption process. The adsorption of the pollutant on the catalyst surface is one of the important factors in photocatalysis (Li et al. 2016). Generally, the organic pollutant adsorption on the photocatalyst surface depends on two factors: the electrical charge of the surface and the electrical charge of the organic pollutant molecules. Therefore, the adsorption capacity of the photocatalyst is known to be pH-dependent (Grzechulska &Morawski 2002). In this work, the adsorption process refers to the adsorption of organic pollutant molecules on the catalyst surface during the photocatalytic reaction.

As seen in Tables 4 and 5, the values of the rate constants for the adsorption step indicate the following comments. (1) The pollutant adsorption on the surface of the photocatalyst under visible light irradiation plays a more prominent role in the degradation process; (2) the amount of TC adsorbed on the N-TiO_2/RGO surface was high in the dark (without light) due to the presence of the RGO; (3) the pre-adsorption of the pollutant on the TiO_2 surface is an essential factor to initiate the photodegradation process under visible light; (4) based on the mechanism proposed in Table 5, TC adsorbed on the TiO_2 surface can be an important factor for the transfer of electrons to the TiO_2 conduction band (Li et al. 2014). These observations are in agreement with the experimental results.

However, the fitting results indicate the critical role of the AOPs in the high degradation of the pollutants. The following possible reasons can be used to explain these results: (1) the powerful holes are produced in the photocatalyst/UV-light system that can rapidly oxidize the pollutants. Therefore, adsorption seems to be less important in these conditions. The experimental results show that only 3.51% of the CR concentration and 5.31% of the AO7 concentration were decreased during the dark adsorption (Han et al. 2018, Peng et al. 2019).

However, the nature of the dark adsorption is different from the adsorption process during the photocatalytic reaction. If organic pollutant molecules were adsorbed on the photocatalyst

surface, they might be more easily oxidized by the valance band holes or ROSs (Hossain et al. 2018). The adsorption step of organic pollutant on the TiO_2 surface is one of the elementary reactions of photocatalytic degradation in the proposed mechanism. Here, it is assumed that the reactive-centers are the sites where the reaction can take place on the catalyst surface. The strategy considered for the adsorption process in the proposed approach can be described as follows: " the degradation of the adsorbed pollutant after light irradiation and then the adsorption of new molecules on the photocatalyst surface."

The trend of changes in the concentration of the adsorption sites obtained from the fitting process can be observed in Figure 3. In agreement with the literature (Yoneyama &Torimoto 2000, Yu et al. 2000), the fitting results indicate that increasing the number of adsorption sites improves the pollutant degradation on the photocatalyst surface. A relative correlation is observed between the degradation efficiency and the adsorption of the pollutant on the photocatalyst surface. The enhanced photocatalytic performance of the 3 wt.% Fe-doped TiO_2 (100 $mg.L^{-1}$, pH=3), 3 wt.% Ni-doped ZnO, and N-doped TiO_2/RGO compared to the other samples could be ascribed to the adsorption ability increasing of these catalysts. In agreement with the experimental results, the effective concentration of adsorption sites in N-doped TiO_2/RGO is increased in virtue of the presence of RGO.

It was found (Sathishkumar et al. 2011) that the catalysts with the higher surface areas provide more reactive-centers, which could increase the organic pollutant adsorption and the incident UV-light on the TiO_2 surface. Since more charge carriers will be generated when the catalyst surface interacts with more photons, the effective photon concentration is maximum in these samples (Figure 3). Therefore, the surface area increasing can lead to high photocatalytic activity and improved pollutant degradation efficiency.

However, the fitting process indicates that the relatively small changes in the rate constant of the adsorption step have a significant effect on the fitting results. One

possible reason for this behavior is the strong effect of the adsorption sites concentration on the photodegradation process.

3.2.4. The effect of the modification of the photocatalyst on the degradation process

The various studies clearly show the doping of semiconductors with non-metallic atoms, transition metals, and organic compounds play a vital role in their photocatalytic performance (Gomez-Ruiz et al. 2018, Haque et al. 2013, Kumar et al. 2016). These strategies are proposed to overcome the limitations of semiconductors, prevent the recombination of the electron-hole pairs, and improve the ROSs production process. By implementing the above strategies, the photocatalytic system provides several possible paths to achieve these goals.

The fitting results show the modification of the TiO_2 and ZnO by the different materials, such as the Fe, Ni, Ag, and RGO leads to the following beneficial effects in the photocatalyst: (1) higher surface area; (2) the more effective trapping of the carriers; (3) the narrowing of the bandgap; (4) the increasing the concentration of water species and oxygen molecules on the photocatalyst surface. These results are in agreement with the experimental findings. The incorporating the nickel into the zinc lattice produces more electron-hole pairs without altering the crystal structure of the ZnO (Gnanamozhi et al. 2020).

The Fe and Ni dopant introduce the impurity states in the band gap of the TiO_2 and ZnO. Also, silver acts as an acceptor material to alter ZnO band gap energy. The results of the X-ray spectroscopy (DRS) showed the band gap of the TiO_2 is narrowed by the N-doping (Peighambardoust et al. 2018). Besides, the coupling of the TiO_2 with RGO decreases the bandgap energy (Li et al. 2020). Therefore, the doping process in these semiconductors leads to a decrease in their bandgap energy. The narrowing of the bandgap increases the efficiency of these photocatalysts for using the visible part of the solar spectrum in pollutants degradation.

Chen et al. (Chen et al. 2015) observed that an appropriate amount of Fe^{3+} ions could act as the reactive-centers for trapping of the charge carriers on the TiO_2 surface. Reddy et al. (Reddy et al. 2018) showed the doping of the Ni^{2+} ions into ZnO lattice improves the interfacial charge transfer by the red shift in Fermi level position. Wageh et al. (Wageh et al. 2018) showed the rate constant of 7% wt. Ag-doped ZnO for the photocatalytic degradation of methyl orange was 38 times more than pure ZnO. They attributed this Ag-doped ZnO behavior to enhanced absorption in visible-light range and improved interfacial charge transfer. Beltrán et al. (Garrafa-Gálvez et al. 2019) found the photocatalytic performance of the TiO_2/RGO nanocomposite under solar light irradiation was ~5 times that of pure TiO_2. The improvement of the photocatalytic activity of the TiO_2/RGO was attributed to RGO role as a charges transporter and accepter.

Therefore, the degradation rate increases by modifying the TiO_2 and ZnO due to these important factors: (1) it leads to more effective separation of the hole-electron pairs, and (2) the synergistic effects between the new materials and semiconductors are seen. In other words, the dopants (Fe, Ni, Ag) and the RGO can form intermediate pathways for the transport and interfacial transfer of charge carriers. Therefore, this proposed approach uses many pathways for the degradation of pollutants.

$$Fe^{3+}\text{or}Ag + e^- \rightarrow Fe^{2+}\text{or } Ag^- \quad (9)$$

$$Fe^{2+}\text{or } Ag^- + O_2(ads) \rightarrow Fe^{2+}\text{or } Ag^- - O_2(ads) \quad (10)$$

$$Fe^{2+}\text{or } Ag^- - O_2(ads) \rightarrow Fe^{3+}\text{or } Ag + O_2^{-\bullet}(ads) \quad (11)$$

$$Fe^{3+}, Ni^{2+}\text{or RGO} + O_2(ads) \rightarrow Fe^{3+}, Ni^{2+}\text{or RGO} - O_2(ads) \quad (12)$$

$$Fe^{3+}, Ni^{2+}\text{or RGO} - O_2(ads) + e^- \rightarrow Fe^{2+},\ Ni^{+}\text{ or RGO}^- - O_2(ads) \quad (13)$$

$$Fe^{2+},\ Ni^{+}\text{ or RGO}^- - O_2(ads) \rightarrow Fe^{3+}, Ni^{2+}\text{or RGO} + O_2^{-\bullet}(ads) \quad (14)$$

$$Fe^{3+}, Ni^{2+}\text{or Ag} + \text{water species}\left(OH^-(ads)\right) \rightarrow Fe^{3+}, Ni^{2+}\text{or Ag} - OH^-(ads) \quad (15)$$

$$Fe^{3+}, Ni^{2+} \text{or } Ag - OH^{-}(ads) + h^{+} \rightarrow Fe^{3+}, Ni^{2+} \text{or } Ag - OH^{\bullet}(ads) \quad (16)$$

$$Fe^{3+}, Ni^{2+} \text{or } Ag - OH^{\bullet}(ads) \rightarrow Fe^{3+}, Ni^{2+} \text{or } Ag + OH^{\bullet}(ads) \quad (17)$$

Based on these pathways, the concentration of the reactive centers for the studied systems are plotted in Figure 3. This figure indicates the effective concentration of reactive-centers in 3 wt.% Fe-doped TiO_2, 3 wt.% Ni-doped ZnO, N-doped TiO_2/RGO is higher than that of the other samples of their groups. The experimental and fitted results show that the increase of the photocatalytic efficiency of these samples can be attributed to the modification effect of the semiconductors.

3.2.5. The reactions of the charge carriers (the trapping process)

The third part of the proposed mechanism is a set of reactions in which the photogenerated charge carriers participate. The trapped charge carriers exhibit a longer lifetime than the free electrons and holes. Therefore, they can play a more helpful role in the pollutant destruction process. Our approach is based on the trapping of the charge carriers on the surface or in the bulk of a catalyst. A small number of these charges leads to ROSs production, so it was preferred to divide the effective reactive-centers into two categories.

Reactive centers such as RC1, RC2, RC3, RC4, RC5, and RC6 play a prominent role in the generation of the used ROSs in the destruction of organic pollutants. The reactive centers like RC7, RC8, and RC9 (semi-effective centers) prevent the recombination process of the electron-hole pairs. The second type of the centers in bulk or on the surface can trap the charge carriers as follows:

$$e^{-} + S1_{trap} \rightarrow e_{trap} \quad (18)$$

$$h^{+} + S2_{trap} \rightarrow h_{trap} \quad (19)$$

As shown in Table 4, the fitting results showed the rate constant for the Eq. (18) is slightly higher than the rate constant of Eq. (19). However, the rate constant of the holes' trapping by

the first type of the effective reactive-centers has more significant effect on the conformity of the simulated results and experimental data. This result can be ascribed to the higher power of hydroxyl radicals generated by the valance band holes.

Water species are a crucial factor in forming some reactive-centers on the surface of the TiO_2 and ZnO. In the proposed approach, water is adsorbed on the TiO_2 surface in two forms, i.e., the dissociative and the molecular. In molecular adsorption, the oxygen atom electrostatically interacts with a Ti_{5c} site, and the hydrogens form the H bonds with two surface O_{2c} sites on the next ridge. The formation of the hydrogen bonds between water molecules and the TiO_2 surface expands a strong network of high-ordered configurations (Mattioli et al. 2008). In dissociative adsorption, the hydroxyl group bonds to a Ti_{5c} atom, and hydrogen ion bonds to an O_{2c} atom. Therefore, two distinct hydroxyl groups can arise from the water dissociation on the TiO_2 surface, i.e., terminal and bridging hydroxyl species (Patrick &Giustino 2014, Wahab et al. 2008). Because the 5-fold coordinated Ti atoms act as Lewis acid sites able to form powerful bonds with electron pairs of water molecules, and 2-fold coordinated oxygen atoms act as Lewis base sites able to share a pair of the electrons with empty orbitals. Walle et al. (Walle et al. 2011) showed that the amount of molecular and dissociated species of the adsorbed water on the surface are comparable. Dissociative adsorption of water molecules can produce hydroxyl groups and protons bonded to the TiO_2 surface. The hydrogen and hydroxyl ions of the aqueous solution are adsorbed on the TiO_2 surface and create the reactive-centers of the RC1. On the other hand, the interaction of water species and Fe^{3+} and Ni^{2+} ions leads to the formation of the RC2 reactive-centers on the surface of the Fe-doped TiO_2 and Ni-doped ZnO. It was reported (Carneiro et al. 2011) that the iron doping into the TiO_2 lattice leads to more surface hydroxylation.

In the past decades, the water interaction with the ZnO surface has been studied using both experimental and computational methods. Martins et al (Martins et al. 1996) investigated the

adsorption of the H_2O molecules on a $(ZnO)_{22}$ cluster by using some semi-empirical procedures. Their results indicated the weak interaction of the hydrogen atom of water with the oxygen atom of the ZnO surface leads to the formation of the O-H ....O band.

Kharche et al. (Kharche et al. 2014) analyzed the microscopic structure of the ZnO aqueous interfaces using the first-principles density functional theory. They concluded that protons of the dissociated water molecules interact with the oxygen anions of the ZnO surface, while the hydroxide ions interact with Zn cations. The presence of hydroxyl groups is confirmed by the FT-IR spectroscopy (Gnanamozhi et al. 2020). The interaction of H_2O molecule with the oxygen-terminated polar surface of ZnO was investigated by Kunat et al (Kunat et al. 2003). They suggested that two OH-species are formed by the dissociation of water molecules at the O-vacancy. Therefore, water is adsorbed on the ZnO surface in both physisorption and chemisorption forms (Nagao 1971, Yue et al. 2018).

The FT-IR spectra exhibit the presence of Zn-O-Ni bonds for all the Ni-doped ZnO samples (Mousavi et al. 2017). Water molecules and hydroxyl ions can interact with nickel ions on the Ni-doped ZnO surface to form the reactive-centers of the RC2 (Assowe et al. 2012, Cappus et al. 1993, Simion et al. 2017). According to the proposed approach, these reactive-centers have a synergistic effect on the organic pollutant photodegradation. The concentrations of the reactive- centers are considered as a function of the pH solution. At the isoelectric point, the molecular form of water is effective in the formation of the reactive-centers due to the low concentration of hydroxyl and hydrogen ions.

Since the report of the photocatalysis phenomena, many authors (Montoya et al. 2013, Salvador 2007) confirmed that electrons and holes are trapped in bulk or on the surface of photocatalyst. It has been debated whether the VB free holes are trapped by surface-adsorbed water species, or by the surface oxygen ions (Liu et al. 2014). The analysis of the electronic structure showed (Bahnemann et al. 1984) the HOMO levels of the adsorbed water on the rutile

TiO_2 (110) are much less than the top of the TiO_2 VB level. For this reason, Salvador (Salvador 2007) explained the photogenerated holes do not have enough power to oxidize the adsorbed water species, and the oxidation of the water molecules by photogenerated holes is prohibited. The photo-induction process may change the position of the molecular orbitals in the electronic structure of the adsorbed water species. Therefore, some authors still believe the photocatalytic process is initiated through the oxidation of the adsorbed water on the surface by the valence band holes (Tan et al. 2012).

The formation of surface-adsorbed hydroxyls in the $A-\text{doped}\ M_xO_y$ photocatalyst can be written as follows:

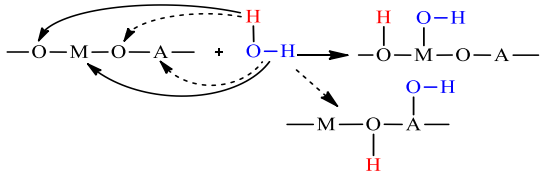

(20)

Photo-induced holes generated under UV illumination are simultaneously trapped with the conduction band electrons (Bahnemann et al. 1997). The trapped hole on the surface is considered as an adsorbed $OH^{\bullet}$ radical (Nosaka &Nosaka 2017, Schneider et al. 2014). The holes trapped are transferred to water species, resulting in the formation of $OH^{\bullet}(ads)$. Researchers believe the hydroxyl radicals or the surface-adsorbed holes are the main oxidizing intermediates for the degradation of the organic pollutants (Andreozzi et al. 1999, Kuang et al. 2016). Several groups were presented the experimental evidence of the production of hydroxyl radical in photocatalytic reactions (Al-Ekabi et al. 1989, Carraway et al. 1994, Mao et al. 1991, Okamoto et al. 1985). Hydroxyl radicals ($OH^{\bullet}$) are short-lived and strong oxidants in an aqueous medium that react quickly with many of the dissolved compounds. The reaction between ROSs and an organic pollutant is symbolically represented in the fourth part of the general mechanism.

According to the experimental conditions, it has been reported (Qian et al. 2019) the trapping timescale of the VB holes varies between picosecond and nanosecond. As shown in Table 4, the rate constants of the trapping the valance band holes by the reactive-centers of RC1 or RC2 are in order 10^9. Our findings show a good correlation between the rate constant and the timescale of the trapping process. The trapping step of VB holes is the most important step of pollutant degradation due to the high reactivity of hydroxyl radicals (Munter 2001). The fitting results showed that the rate constant of the hole trapping step by the reactive-centers has a significant impact on the fitting curve.

Therefore, it is easy to understand the importance of water species and dopant level in the photocatalytic degradation of the pollutant using the proposed mechanism. As shown in Figure 3a, the fitting results indicate that the effective concentration of reactive-centers of the RC1, and RC2 are at their maximum value in a sample with the highest photocatalytic performance. Therefore, these variables can be used to find the optimal condition of the studied system.

An important pathway for the organic pollutant oxidation in photocatalytic reactions is the direct attack of VB holes to the pollutant molecules adsorbed on the catalyst surface. This step competes with the reaction of hydroxyl radicals and the pollutant molecules, because these charges have high oxidation potential (2.9 V vs. SHE in pH=0). The main pathway of the organic pollutant degradation is determined by the type of the catalyst and the pollutant's nature. However, the fitting results confirm the adsorbed pollutants on the TiO_2 surface are destroyed by the direct attack of the VB holes, and the rate constant of this step affects the fitting curve.

Chen et al. (Chen et al. 2005) indicated the AO7 degradation is primarily initiates by photo-induced holes. Sivalingama et al. (Sivalingam et al. 2003) investigated the photocatalytic degradation of the various dyes in the TiO_2 suspension under UV light irradiation. They assumed that dyes are oxidized by direct attacks of holes and hydroxyl radicals. Bahnemann et

al. (Bahnemann et al. 1997) found a mechanism for the photocatalytic oxidation of dichloroacetate and thiocyanate on the TiO_2 (anatase). They stated the strongly-adsorbed molecules react with the free VB holes, whereas the weakly-adsorbed species react with long-live trapped holes.

The adjusted value of the rate constant (Table 4) shows the rate of this step is comparable with the trapping the holes in the reactive-centers of RC1 and RC2. In other words, the rate constant confirms the claim that direct attack of holes supports the pollutants destruction by hydroxyl radicals. The computational results demonstrate that the rate constant of this step has a lower effect on the fitting process than the trapping of the holes by the reactive-centers of RC1 and RC2. Therefore, there are two distinct pathways for the degradation of organic pollutant: (1) the free- degradation by the charges trapped on the photocatalyst surface, and (2) degradation of pollutants absorbed on the surface of the photocatalyst by free holes . The role of these pathways in eliminating of pollutants depends on the photocatalyst nature, the pollutant structure, and the solution pH. The fitting results indicate the second pathway is less important because its proceeding depends on the adsorption reaction. One possible reason is that reactive-centers are more accessible than adsorbed molecules.

The photogenerated holes have a short life-time, which can attack and destroy the adsorbed dye molecules on the photocatalyst surface. The intermediates produced during the AO7 photodegradation process may be adsorbed on the photocatalyst surface or diffuse into the solution. It is possible that the absorbed intermediate molecules on the surface are destroyed by the free VB holes. However, the simulation results show that the reaction of the photogenerated holes with intermediates has no effect on the AO7 degradation process. In other words, the curve of the AO7 concentration versus time is not affected by a change in the rate constant of this reaction. Therefore, the reaction of the photo-induced holes with intermediate molecules was ignored in the proposed mechanism.

On the other hand, excess electrons are usually available on the photocatalyst surface due to various factors such as intrinsic defects, the other element doping into the TiO_2 lattice, and the photo-induction by UV/Vis light illumination. These electrons may be trapped by some adsorbed species on the photocatalyst surface.

Oxygen molecules can play an essential role in the formation of the reactive-centers. The ability of the charged oxygen molecules production is an influential factor in photoactivity. Wu et al. (Wu et al. 2003) suggested two molecular and one dissociated adsorbed configurations for the O_2 adsorption on the TiO_2 surface. In the most stable molecular configuration, the oxygen molecule is adsorbed on the vacancy site, and binds to the two nearest Ti cations. In the other molecular configuration, O_2 molecule is located on top of a Ti_{5c} atom. The binding energy of this configuration is ~2 eV smaller than the binding energy of the first configuration.

Due to the availability of adequate oxygen, our approach assumes the O_2 molecules primarily adsorb on the $A-\text{doped } M_xO_y/B$ surface, leading to the formation of RC3, RC4, and RC5. These reactive-centers trap the excess electrons. When the photogenerated holes quickly migrate to the surface trapping centers, electrons are initially trapped in Ti^{4+} lattice trapping states (Di Valentin et al. 2006). The photoexcited electrons in Ti^{3+} defect sites were firmly confirmed by the electron paramagnetic resonance (EPR) technique (Hurum et al. 2003). The transfer of one or more trapped electrons to the oxygen molecules leads to the formation of adsorbed-surface oxygen, and consequently, the generation of the superoxide anion radicals. It was reported (Fujishima et al. 2008) the trapped electrons react with oxygen molecules faster than the free electrons.

Superoxide radicals ($O_2^{\bullet-}$) enable to act as the effective species for destroying many toxic organic pollutants (Carter et al. 2007, Ryu &Choi 2004). Kuang et al (Kuang et al. 2016) found that 40% of the total degradation of orange II and methylene blue dyes could be attributed to $^1O_2$, $O_2^{\bullet-}$ and the UV photolysis in the TiO_2/UV system. The formation of $O_2^{\bullet-}$ during the

photocatalytic reactions was confirmed by several techniques (Jaeger &Bard 1979, Nosaka et al. 1997). The characteristic time for trapping of the charge carriers varies depending on the experimental conditions from picosecond to nanosecond timescale (Friedmann et al. 2010). Tamaki et al. (Tamaki et al. 2007) reported that the electrons and holes are trapped on the surface of the anatase TiO_2 at ~200 fs timescale.

Bahnemann et al. (Bahnemann et al. 1997) determined a rate constant of the reaction of the trapped electrons with oxygen molecules as 7.6×10^7 $L.mol^{-1}.s^{-1}$. Gerischer (Gerischer 1995) reported the rate constants for transfer of free and trapped electrons to oxygen molecules are 4.5×10^7 s^{-1} and 4.5×10^3 s^{-1}, respectively.

In our study, it is assumed the concentration of dissolved oxygen (DO) remains constant during the photocatalytic reaction. Pan et al. (Li et al. 2019) investigated the various properties of the ZnO nanoparticle as a gas sensor. They found that oxygen molecules are rapidly pre-adsorbed on the surface of the ZnO (001). Wang et al. (Li et al. 2005) studied the sensing mechanism of the ZnO films by the transient photocurrent technique. Their results indicated that O_2 molecules are adsorbed on the surface of ZnO in both physisorption and chemisorption forms. When the Ni-doped ZnO is exposed to oxygen, the reactive-centers of the Ni-O_2 are formed by the reaction of the adsorbed oxygen molecules with nickel ions (Norton et al. 1977, Qian et al. 2020).

In our provided mechanism, the photogenerated electrons are trapped by Ti^{4+}, Fe^{3+}, Zn^{2+}, and Ni^{2+} ions in the reactive-centers of $Ti^{4+}-O_2(ads)$, $Fe^{3+}-O_2(ads)$, $Zn^{2+}-O_2(ads)$, $Ni^{2+}-O_2(ads)$, and $RGO-O_2(ads)$. Besides, silver is considered as a reactive-center, which can accept and transfer the CB electrons of the semiconductor. Some studies (Sengunthar et al. 2020, Yu et al. 2018) showed the higher photocatalytic efficiency of RGO/TiO_2 and RGO/ZnO is attributed to RGO. It acts as (1) a charge separator, (2) a photosensitizer, and (3) a good

adsorbent. The RGO sheets transfer the CB electrons to the adsorbed oxygen molecules on the nanocomposite surface to produce $O_2^{\bullet-}$ radicals.

As shown in Figure 3c, the improvement of the photocatalytic efficiency of the N-doped TiO_2/RGO sample can be attributed to the presence of RC5 reactive-centers, which can trap the CB electrons. The fitting results show the rate constant of the trapping of photo-induced electrons by the reactive-centers of the RC3, RC4, and RC5 is in the order of 10^9. The values of the rate constants are consistent with this strategy and to the timescale of the process of trapping the CB electrons on the TiO_2 surface (Friedmann et al. 2010).

The results of our work show the fitting process is affected by changing the value of the rate constant for the reaction of the CB electrons with the reactive-centers of the RC3, RC4, and RC5. Therefore, using the proposed mechanism, the role of the following two factors in the pollutants photodegradation can be explained: (1) the synergistic effect of the Fe^{3+}, Ni^{2+}, RGO, and Ag^+ with TiO_2 and ZnO, and (2) the flow rate of the O_2.

The proposed mechanism is in good agreement with the experimental results. Trapping experiments showed that $OH^{\bullet}$and $O_2^{\bullet-}$ in the system of the Ag/ZnO/O_3/Phenol plays a major role in the degradation of pollutants, which is consistent with the EPR results (Peng et al. 2019). On the other hand, the radical quenching experiments clearly indicated that $O_2^{\bullet-}$ radicals have an important role in the TC photodegradation under visible light illumination (Tang et al. 2018).

Hydrogen peroxide (H_2O_2) is another important ROSs in photocatalytic systems. It is produced from two pathways during the photocatalytic processes. Those are the two-hole oxidation of H_2O and the two-electron reduction of O_2(ads) (Hirakawa et al. 2001, Nosaka &Nosaka 2017, Sahel et al. 2016), as follows:

$$2\,H_2O + 2\,h^+ \longrightarrow H_2O_2 + 2H^+ \quad (21)$$

$$O_2^{\bullet-} + e^- + 2\,H^+ \longrightarrow H_2O_2 \quad (22)$$

The reduction pathway seems to be dominant due to the low reactivity of superoxide radicals. Li and Selloni (Li &Selloni 2013) found the generation of $O_2^{\bullet-}$ via the transfer of an electron to an oxygen molecule is barrier-less. In contrast, the transfer of the second electron to adsorbed superoxide to produce an adsorbed H_2O_2 is nonadiabatic, and it has a barrier of 0.3eV at the anatase TiO_2. A low concentration of hydrogen peroxide has been detected in the aqueous suspension of the TiO_2 and ZnO under UV illumination (Mrowetz &Selli 2006, Nosaka et al. 1997). It can be formed by the reaction of the electrons with superoxide radicals in the presence of protons (Sahel et al. 2016):

$$O_2^{-\bullet}(ads) + e^- + 2H^+ \rightarrow H_2O_2(ads) \quad (23)$$

It was reported (Nosaka &Nosaka 2017) the quantum yield of the H_2O_2 generation is in the order of 10^{-7} for the TiO_2 powder, and in the order of 10^{-3} for the anatase TiO_2 films. Although the rate constant of this reaction is high, the fitting results show that this reaction has little effect on the fitting curve. The reason may be as follows: (1) the proceeding of this reaction depends on the presence of three species; (2) the concentration of hydrogen ions is low in the non-acidic solution.

The rate constant for the reaction of the aqueous electrons with H_2O_2 is in the order of 10^{10} $M^{-1}. s^{-1}$ (Gierer et al. 1994). This reaction is thermodynamically favorable (ΔE^0 = +0.73 V at pH 7) (Nosaka &Nosaka 2017). The fitting results show the adjusted value of the rate constant for the electron reaction with H_2O_2 is in the order of 10^9. This result is consistent with the trapping process of the CB electrons on the TiO_2 surface. Therefore, the reaction of electrons with H_2O_2 has a significant effect on degradation of organic pollutant. As a result, the effect of H_2O_2 on the degradation process in photocatalytic systems can be investigated with these explanations.

3.2.6. The recombination of the charge carriers

The sixth part of the general mechanism is the recombination of the charge carriers. In our approach, the degradation of the organic pollutants is prevented by both recombinations of the free and the trapped electron-hole pairs. The trapping of the charge carriers not only prevents the recombination process but also increased the carriers lifetime. As seen in Table 4, the value of the rate constant is in the order of 10^9 for this step. In this work, the effect of the recombination of the charge carriers on the fitting process was investigated by changing the value of the rate constant. The fitting results show that the recombination of e^-/h^+ pairs has a determining role in the degradation of the organic pollutant. The recombination of the charge carriers is an important step of the photodegradation process that occurs in a femtosecond timescale. The quantum yields of the most photocatalytic reactions are less than 10%, and it can be due to the recombination process. After a certain time, the charge carriers are recombined to produce light and heat. The recombination of the charge carriers is one of the most important factors in the fabrication of photocatalysts and the design of the photoreactors (Li &Li 2002, Visan et al. 2019, Wang et al. 2010).

The adjusted value of the rate constant for the recombination of the charge carriers shows that this step has a significant effect on the degradation process of organic pollutants. Besides, the fitting results indicate the following findings: (1) the free charge carriers recombine faster than the charge carriers trapped by the TiO_2 surface; (2) the value of R^2 changes significantly by changing the value of the rate constant for the trapping of the CB electrons by the semi-effective centers; (3) the fitting process is strongly influenced by the recombination of the charge carriers trapped in the reactive-centers.

Figure 3 shows that the concentration of the semi-effective centers is highest in the following samples: 3% wt. Fe-doped TiO_2, pH=3, 3% wt. Ni-doped ZnO, N-doped TiO_2/RGO, and Ag-doped ZnO/O_3. The fitting results are in agreement with the experimental results. Using the proposed approach, a deeper understanding of the recombination process is obtained, and

the obtained results are in agreement with the previous studies (Krýsa et al. 2006, Qian et al. 2019, Rothenberger et al. 1985). Therefore, this study confirms the trapping of the charge carriers by the active sites is an acceptable strategy.

3.2.7. Inactivation reactive-centers

A prominent feature of the proposed mechanism is that hydroxyl radicals are consumed by the inactivation of the reactive-centers (Barka et al. 2010, Daneshvar et al. 2004, Dutta et al. 2009). This step is symbolically represented in the seventh part of the general mechanism (Table 3). The nature of these centers is highly dependent on the type of catalyst and the reaction conditions. For instance, the following two reactions can be performed to form H_2O_2 (Guo et al. 2011, Pelizzetti &Minero 1993):

$$TiO^{\bullet}H + TiO^{\bullet}H \rightarrow H_2O_2(ads) \quad (24)$$

$$TiO^{\bullet}H + OH^- \rightarrow H_2O_2(ads) + e^- \quad (25)$$

Daneshvar et al. (Daneshvar et al. 2004) and Dutta et al. (Dutta et al. 2009) assumed the hydroxyl radicals produced in the photocatalytic reaction could be consumed by the inactivation species. They suggested that inactivation of the hydroxyl radicals with inactive-centers is more important than other steps. According to Table 4, the fitting results show that the rate constant of the inactivation step is in the order of 10^6. This study shows the fitting data is affected by changing the value of the rate constant for the reaction of the inactivation species with the ROSs. Therefore, this step has an essential impact on the degradation of the pollutant and competes with other reactions.

On the other hand, some inactivated $OH^{\bullet}$ radicals may be reactivated by the participation of water molecules and activation sites. For example, the produced H_2O_2 in the photocatalytic reaction may be converted to hydroxyl radicals by the following reactions:

$$Ti^{IV} + e^- + H_2O \rightarrow Ti^{III}OH_2 \quad (26)$$

$$Ti^{III}OH_2 + H_2O_2(ads) \rightarrow TiO^{\bullet}H + OH^- + Ti^{IV}OH_2 \quad (27)$$

In this work, the effect of the re-activation step on the degradation of the organic pollutant was investigated by changing the values of the rate constants. The results indicated that the reactivation process in the studied systems is much less important than the generation of hydroxyl radicals or the inactivation reaction. For this reason, the reactivation steps were omitted in the final mechanism.

3.2.8. Comparison of the pollutants photodegradation caused by different light sources

This approach can be used to investigate the photodegradation mechanism of the organic pollutants by photocatalysts with the general formula A-doped M_xO_y under different irradiation sources. In this work, the AO7 photodegradation on the 2wt.% Fe-doped TiO_2 surface induced by different light sources was simulated. The curves of the AO7 concentration versus time for these samples is plotted in Figure (5). As can be seen in this figure, there is good conformity between the results of the simulation and the experimental data. The adjusted values of the rate constants of the first step for the irradiation sources of the UV-, solar-, and visible-light are: 1.47×10^{-3}, 7.33×10^{-4}, and 4.90×10^{-4} $M^{-1}.min^{-1}$. The rate constant of the other steps is the same as the values given in Table (2) for the Fe-doped TiO_2 system. These results show the degradation efficiency of the UV-light is greater than that of the solar-light and visible-light. The simulation results show the effective concentration of photons (I_{eff}) in the 2wt.% Fe-doped TiO_2/visible-light/AO7 system is lower than other samples. The reason can be attributed to the lower power of visible-light photons. This decreases the effective concentration of the charge carriers and thus the rate of the AO7 degradation.

We predict the proposed approach can also be used to investigate the mechanism and kinetics of photocatalytic reactions using other photocatalysts such as sulfides. However, it should be examined in another study.

4. Conclusion

In this study, a new approach and a general mechanism are provided to investigate the kinetics of the degradation of the organic pollutants by the photocatalysts under UV/Vis light irradiation. This approach was examined to find a suitable mechanism for the photodegradation of the four different empirical systems of acid orange 7 on Fe^{3+}-doped TiO_2 nanocatalysts, ozonation of phenol on Ag/ZnO nanocomposites, tetracycline hydrochloride on N-doped TiO_2/reduced graphene oxide, and congo Red on Ni-doped ZnO. The production of the effective reactive-centers and the trapping of the charge carriers are two main strategies used in the proposed mechanism. This mechanism describes the experimental data well, and it can be used to predict the behavior of the photocatalytic systems at different conditions. The fitting results showed the excellent conformities between the calculated and experimental data at various conditions.

Two methods were used to estimate the parameters: the hybrid manual-automatic method and the optimization-based techniques. The first method can be performed in two steps to obtain good agreement between the experimental data and the fitting results: (1) manual adjusting the system parameters, and (2) the optimization by the $fminsearch$ function. The fitting results show the hybrid manual-automatic method leads to reliable values than optimization-based procedure. Moreover, the fitting results showed:

(1) the rate constant of electron-hole generation step in the proposed mechanism is in the order of 10^{-3} for UV-light and 10^{-1} for visible light illumination. Therefore, a small fraction of the charge carriers can lead to the degradation of the organic pollutants;

(2) the photocatalyst surface is composed of the different reactive-centers in contact to the water species and the other materials. Depending on the reaction conditions, a certain number of these centers participate in the organic pollutants degradation. The synergic effect of dopants

increases the surface area, the effective reactive-centers, and the trapped e^-/h^+ pairs, and thus, it improves the pollutants photodegradation;

(3) the photodegradation efficiency is highest when the effective concentration of the reactive-centers and the effective concentration of photons are maximum. Therefore, the optimum conditions can be achieved by the plotting of the concentration curve of the reactive-centers for different conditions;

(4) the hydroxyl radicals and superoxide radicals are mainly responsible for the degradation of the organic pollutants;

The proposed mechanism in this work can be utilized to construct efficient photocatalysts, to study the kinetics of the organic pollutants photodegradation on the surface, and to optimize them.

Availability of data and materials

The datasets used and/or analyzed during the current study are available from the corresponding author on reasonable request.

All data generated or analyzed during this study are included in this published article [and its supplementary information files].

Ethics approval and consent to participate

Not applicable.

Consent for publication

Not applicable.

Authors' contributions

Conception and design of study: H. Bashiri; M. Arabameri

Collected the data, analysis and/or interpretation of data: M. Arabameri

Wrote the manuscript: M. Arabameri; H. Bashiri

All authors read and approved the final manuscript.

Acknowledgement

The authors are grateful to University of Kashan for supporting this work by Grant No. (1073182/3).

Competing of interests

☒ The authors declare that they have no known competing financial interests or personal relationships that could have appeared to influence the work reported in this paper.

☒The authors declare the following financial interests/personal relationships which may be considered as potential competing interests:

References:

Al-Ekabi H, Serpone N, Pelizzetti E, Minero C, Fox MA, Draper RB (1989): Kinetic studies in heterogeneous photocatalysis. 2. Titania-mediated degradation of 4-chlorophenol alone and in a three-component mixture of 4-chlorophenol, 2, 4-dichlorophenol, and -5 ,4 ,2trichlorophenol in air-equilibrated aqueous media. Langmuir 5: 250-255

Al-Kdasi A, Idris A, Saed K, Guan CT (2004): Treatment of textile wastewater by advanced oxidation processes—a review. Global nest: the Int. J 6: 222-230

Al-Rasheed RA (2005): Water treatment by heterogeneous photocatalysis an overview, 4th SWCC acquired Experience Symposium held in Jeddah, pp. 1-14

Alkaim A, Aljeboree A, Alrazaq N, Baqir S, Hussein F, Lilo A (2014): Effect of pH on adsorption and photocatalytic degradation efficiency of different catalysts on removal of methylene blue. Asian J. Chem. 26: 8445

Andreozzi R, Caprio V, Insola A, Marotta R (1999): Advanced oxidation processes (AOP) for water purification and recovery. Catal. Today 53: 51-59

Assowe O, Politano O, Vignal V, Arnoux P, Diawara B (2012): A reactive force field molecular dynamics simulation study of corrosion of nickel, Defect and Diffusion Forum. Trans Tech Publ, pp. 139-145

Bahnemann D, Henglein A, Lilie J, Spanhel L (1984): Flash photolysis observation of the absorption spectra of trapped positive holes and electrons in colloidal titanium dioxide. The Journal of Physical Chemistry 88: 709-711

Bahnemann DW, Hilgendorff M, Memming R (1997): Charge carrier dynamics at TiO_2 particles: reactivity of free and trapped holes. The Journal of Physical Chemistry B 101: 4265-4275

Barka N, Qourzal S, Assabbane A, Ait-Ichou Y (2010): Kinetic modeling of the photocatalytic degradation of methyl orange by supported TiO_2. Journal of Environmental Science and Engineering 4: 1-5

Bashiri H, Jalali HM, Rasa H (2014): Determination of intracellular levels of reactive oxygen species using the 2, 7-dichlorofluorescein diacetate assay by kinetic Monte Carlo simulation. Progress in Reaction Kinetics and Mechanism 39: 281-291

Bashiri H, Mohamadi S (2016): Hydrogen sulfide decomposition on Ni surface: A kinetic Monte Carlo study. Applied Catalysis A: General 509: 105-110

Bashiri H, Pourbeiram N (2016): Biodiesel production through transesterification of soybean oil: A kinetic Monte Carlo study. J. Mol. Liq. 223: 10-15

Berberidou C, Kitsiou V, Karahanidou S, Lambropoulou DA, Kouras A, Kosma CI, Albanis TA, Poulios I (2016): Photocatalytic degradation of the herbicide clopyralid: kinetics, degradation pathways and ecotoxicity evaluation. Journal of Chemical Technology & Biotechnology 91: 2510-2518

Cappus D, Xu C, Ehrlich D, Dillmann B, Ventrice Jr C, Al Shamery K, Kuhlenbeck H, Freund H-J (1993): Hydroxyl groups on oxide surfaces: NiO (100), NiO (111) and Cr_2O_3 (111). Chem. Phys. 533-546 :177

Carneiro JT, Savenije TJ, Moulijn JA, Mul G (2011): How phase composition influences optoelectronic and photocatalytic properties of TiO_2. The Journal of Physical Chemistry C 115: 2211-2217

Carraway ER, Hoffman AJ, Hoffmann MR (1994): Photocatalytic oxidation of organic acids on quantum-sized semiconductor colloids. Environ. Sci. Technol. 28: 786-793

Carter E, Carley AF, Murphy DM (2007): Evidence for O_2-radical stabilization at surface oxygen vacancies on polycrystalline TiO_2. The Journal of Physical Chemistry C 111: 10630-10638

Chakrabarti S, Dutta BK (2004): Photocatalytic degradation of model textile dyes in wastewater using ZnO as semiconductor catalyst. J. Hazard. Mater. 112: 269-278

Chen C-C, Hu S-H, Fu Y-P (2015): Effects of surface hydroxyl group density on the photocatalytic activity of Fe^{3+}-doped TiO_2. J. Alloys Compd. 632: 326-334

Chen Y, Yang S, Wang K, Lou L (2005): Role of primary active species and TiO_2 surface characteristic in UV-illuminated photodegradation of Acid Orange 7 .Journal of Photochemistry and Photobiology A: Chemistry 172: 47-54

Chen Y, Liu K (2016): Preparation and characterization of nitrogen-doped TiO_2/diatomite integrated photocatalytic pellet for the adsorption-degradation of tetracycline hydrochloride using visible light. Chem. Eng. J. 302: 682-696

Daneshvar N, Rabbani M, Modirshahla N, Behnajady M (2004): Kinetic modeling of photocatalytic degradation of Acid Red 27 in UV/TiO_2 process. Journal of Photochemistry and Photobiology A: Chemistry 168: 39-45

Devi LG, Nithya P, Abraham C, Kavitha R (2017): Influence of surface metallic silver deposit and surface fluorination on the photocatalytic activity of rutile TiO_2 for the degradation of crystal violet a cationic dye under UV light irradiation. Materials Today Communications 10: 1-13

Di Valentin C, Pacchioni G, Selloni A (2006): Electronic structure of defect states in hydroxylated and reduced rutile TiO_2 (110) surfaces. Phys. Rev. Lett. 97: 166803

Dou Y, Torralva BR, Allen RE (2004): Interplay of electronic and nuclear degrees of freedom in a femtosecond-scale photochemical reaction. Chem. Phys. Lett. 392: 352-357

Dror I, Fink L, Weiner L, Berkowitz B (2020): Elucidating the catalytic degradation of enrofloxacin by copper oxide nanoparticles through the identification of the reactive oxygen species. Chemosphere 258: 127266

Dutta S, Parsons SA, Bhattacharjee C, Jarvis P, Datta S, Bandyopadhyay S (2009): Kinetic study of adsorption and photo-decolorization of Reactive Red 198 on TiO_2 surface. Chem. Eng. J. 15674-679 :5

El Mragui A, Logvina Y, Pinto da Silva L, Zegaoui O, Esteves da Silva JC (2019): Synthesis of Fe-and Co-doped TiO_2 with improved photocatalytic activity under visible irradiation toward carbamazepine degradation. Materials 12: 3874

Emeline AV, Ryabchuk V, Serpone N (2000): Factors affecting the efficiency of a photocatalyzed process in aqueous metal-oxide dispersions: prospect of distinguishing between two kinetic models. Journal of Photochemistry and Photobiology A: Chemistry 133: 89-97

Forsythe GE (1977): Computer methods for mathematical computations. Prentice-Hall series in automatic computation 259

Friedmann D, Mendive C, Bahnemann D (2010): TiO_2 for water treatment: parameters affecting the kinetics and mechanisms of photocatalysis. Applied Catalysis B: Environmental 99: 398-406

Fujishima A, Zhang X, Tryk DA (2008): TiO_2 photocatalysis and related surface phenomena. Surf. Sci. Rep. 63: 515-582

Galindo C, Jacques P, Kalt A (2000): Photodegradation of the aminoazobenzene acid orange 52 by three advanced oxidation processes: UV/H_2O_2, UV/TiO_2 and VIS/TiO_2: comparative mechanistic and kinetic investigations. Journal of Photochemistry and Photobiology A: Chemistry 130: 35-47

Garrafa-Gálvez HE, Alvarado-Beltrán CG, Almaral-Sánchez JL, Hurtado-Macías A, Garzon-Fontecha AM, Luque PA, Castro-Beltrán A (2019): Graphene role in improved solar photocatalytic performance of TiO_2-RGO nanocomposite. Chem. Phys. 521: 35-43

Gerischer H (1995): Photocatalysis in aqueous solution with small TiO_2 particles and the dependence of the quantum yield on particle size and light intensity. Electrochim. Acta 40: 1277-1281

Ghatak HR (2014): Advanced oxidation processes for the treatment of biorecalcitrant organics in wastewater. Crit. Rev. Environ. Sci. Technol. 44: 1167-1219

Gierer J, Yang E, Reitberger T (1994): On the Significance of the Superoxide Radical in Oxidative Delignification, Studied with 4-t-Butylsyringol and 4-t-Butylguaiacol. Part I. The Mechanism of Aromatic Ring Opening. Holzforschung-International Journal of the Biology, Chemistry, Physics and Technology of Wood 48: 405-414

Gnanamozhi P, Renganathan V, Chen S-M, Pandiyan V, Arockiaraj MA, Alharbi NS, Kadaikunnan S, Khaled JM, Alanzi KF (2020): Influence of Nickel concentration on the photocatalytic dye degradation (methylene blue and reactive red 120) and antibacterial activity of ZnO nanoparticles. Ceram. Int. 46: 18322-18330

Gomez-Ruiz B, Ribao P, Diban N, Rivero MJ, Ortiz I, Urtiaga A (2018): Photocatalytic degradation and mineralization of perfluorooctanoic acid (PFOA) using a composite TiO_2− rGO catalyst. J. Hazard. Mater. 344: 950-957

Grzechulska J, Morawski AW (2002): Photocatalytic decomposition of azo-dye acid black 1 in water over modified titanium dioxide. Applied Catalysis B: Environmental 36: 45-51

Guo MY, Ng AMC, Liu F, Djurišić AB, Chan WK (2011): Photocatalytic activity of metal oxides—the role of holes and OH radicals. Applied Catalysis B: Environmental 107: 150-157

Gupta VK, Jain R, Mittal A, Saleh TA, Nayak A, Agarwal S, Sikarwar S (2012): Photo-catalytic degradation of toxic dye amaranth on TiO_2/UV in aqueous suspensions. Materials Science and Engineering: C 32: 12-17

Han F, Kambala V, Dharmarajan R, Liu Y, Naidu R (2018): Photocatalytic degradation of azo dye acid orange 7 using different light sources over Fe^{3+}-doped TiO_2 nanocatalysts. Environmental Technology & Innovation 12: 27-42

Haque M, Khan A, Umar K, Mir NA, Muneer M, Harada T, Matsumura M (2013): Synthesis, characterization and photocatalytic activity of visible light induced Ni-doped TiO_2. Energy and Environment Focus 2: 73-78

Hirakawa T, Kominami H, Ohtani B, Nosaka Y (2001): Mechanism of photocatalytic production of active oxygens on highly crystalline TiO_2 particles by means of chemiluminescent probing and ESR spectroscopy. The Journal of Physical Chemistry B 105: 6993-6999

Hitam C, Jalil A (2020): A review on exploration of Fe_2O_3 photocatalyst towards degradation of dyes and organic contaminants. Journal of Environmental Management 258: 110050

Hossain MK, Pervez M ,Uddin MJ, Tayyaba S, Mia M, Bashar M, Jewel M, Haque M, Hakim M, Khan MA (2018): Influence of natural dye adsorption on the structural, morphological and optical properties of TiO_2 based photoanode of dye-sensitized solar cell. Materials Science-Poland 93-101 :36

Hu A, Liang R, Zhang X, Kurdi S, Luong D, Huang H, Peng P, Marzbanrad E, Oakes K, Zhou Y (2013): Enhanced photocatalytic degradation of dyes by TiO_2 nanobelts with hierarchical structures. Journal of Photochemistry and Photobiology A: Chemistry 7-15 :256

Huang Y, Wang H, Huang K, Huang D, Yin S, Guo Q (2020): Degradation kinetics and mechanism of 3-Chlorobenzoic acid in anoxic water environment using graphene/TiO_2 as photocatalyst. Environ. Technol. 41: 2165-2179

Hurum DC, Agrios AG, Gray KA, Rajh T, Thurnauer MC (2003): Explaining the enhanced photocatalytic activity of Degussa P25 mixed-phase TiO_2 using EPR. The Journal of Physical Chemistry B 107: 4545-4549

Ibhadon AO, Fitzpatrick P (2013): Heterogeneous photocatalysis: recent advances and applications. Catalysts 3: 189-218

Jaeger CD, Bard AJ (1979): Spin trapping and electron spin resonance detection of radical intermediates in the photodecomposition of water at titanium dioxide particulate systems. Journal of Physical Chemistry 83: 3146-3152

Kaur P, Sud D (2012): Photocatalytic degradation of quinalphos in aqueous TiO_2 suspension: Reaction pathway and identification of intermediates by GC/MS. J. Mol. Catal. A: Chem. 365: 32-38

Kazeminezhad I, Sadollahkhani A (2016): Influence of pH on the photocatalytic activity of ZnO nanoparticles. Journal of Materials Science: Materials in Electronics 27: 4206-4215

Khalifa M, Bidaisee S (2018): The importance of clean water. Sch J Appl Sci Res 1: 17-20

Khan A, Khan R, Waseem A, Iqbal A, Shah ZH (2016): CdS nanocapsules and nanospheres as efficient solar light-driven photocatalysts for degradation of Congo red dye. Inorg. Chem. Commun. 72: 33-41

Kharche N, Hybertsen MS, Muckerman JT (2014): Computational investigation of structural and electronic properties of aqueous interfaces of GaN, ZnO, and a GaN/ZnO alloy. Physical Chemistry Chemical Physics 16: 12057-12066

Krýsa J, Waldner G, Měšťánková H, Jirkovský J, Grabner G (2006): Photocatalytic degradation of model organic pollutants on an immobilized particulate TiO_2 layer:

Roles of adsorption processes and mechanistic complexity. Applied Catalysis B: Environmental 64: 290-301
Kuang L, Zhao Y, Zhang W, Ge S (2016): Roles of Reactive Oxygen Species and Holes in the Photodegradation of Cationic and Anionic Dyes by TiO 2 under UV Irradiation. Journal of Environmental Engineering 142: 04015065
Kumar S, Singh V, Tanwar A (2016): Structural, morphological, optical and photocatalytic properties of Ag-doped ZnO nanoparticles. Journal of Materials Science: Materials in Electronics 27: 2166-2173
Kunat M, Girol SG, Burghaus U, Wöll C (2003): The interaction of water with the oxygen-terminated, polar surface of ZnO. The Journal of Physical Chemistry B 107: 14350-14356
Lai CW, Juan JC, Ko WB, Bee Abd Hamid S (2014): An overview: recent development of titanium oxide nanotubes as photocatalyst for dye degradation. International Journal of Photoenergy 2014
Lau W-J, Ismail AF (2009): Polymeric nanofiltration membranes for textile dye wastewater treatment: preparation, performance evaluation, transport modelling, and fouling control—a review. Desalination 245: 321-348
Lerkkasemsan N 2010: Mechanistic Modeling of Biodiesel Production via Heterogeneous Catalysis, Virginia Tech
Li C, Zhou H, Yang S, Wei L, Han Z, Zhang Y, Pan H (2019): Preadsorption of O_2 on the exposed (001) facets of ZnO nanostructures for enhanced sensing of gaseous acetone. ACS Applied Nano Materials 2: 6144-6151
Li F, Li X (2002): The enhancement of photodegradation efficiency using Pt–TiO_2 catalyst. Chemosphere 48: 1103-1111
Li Q, Gao T, Wang Y, Wang T (2005): Adsorption and desorption of oxygen probed from ZnO nanowire films by photocurrent measurements. Appl. Phys. Lett. 86: 123117
Li R, Song X, Huang Y, Fang Y, Jia M, Ma W (2016): Visible-light photocatalytic degradation of azo dyes in water by Ag_3PO_4: An unusual dependency between adsorption and the degradation rate on pH value. J. Mol. Catal. A: Chem. 421: 57-65
Li S, Chen H, Wang X, Dong X, Huang Y, Guo D (2020): Catalytic degradation of clothianidin with graphene/TiO_2 using a dielectric barrier discharge (DBD) plasma system. Environmental Science and Pollution Research 27: 29599-29611
Li Y-F, Selloni A (2013): Theoretical study of interfacial electron transfer from reduced anatase TiO_2 (101) to adsorbed O_2. Journal of the American Chemical Society 135: 9195-9199
Li Y-F, Zhang W-P, Li X, Yu Y (2014): TiO_2 nanoparticles with high ability for selective adsorption and photodegradation of textile dyes under visible light by feasible preparation. J. Phys. Chem. Solids 75: 86-93
Liang C-Z, Sun S-P, Li F-Y, Ong Y-K, Chung T-S (2014): Treatment of highly concentrated wastewater containing multiple synthetic dyes by a combined process of coagulation/flocculation and nanofiltration. J. Membr. Sci. 469: 306-315
Liu B, Zhao X, Terashima C, Fujishima A, Nakata K (2014): Thermodynamic and kinetic analysis of heterogeneous photocatalysis for semiconductor systems. Physical Chemistry Chemical Physics 16: 8751-8760
Liu G, Li X, Zhao J, Horikoshi S, Hidaka H (2000) :Photooxidation mechanism of dye alizarin red in TiO_2 dispersions under visible illumination: an experimental and theoretical examination. J. Mol. Catal. A: Chem. 153: 221-229
Malakootian M, Nasiri A, Asadipour A, Kargar E (2019): Facile and green synthesis of $ZnFe_2O_4$@ CMC as a new magnetic nanophotocatalyst for ciprofloxacin degradation from aqueous media. Process Safety and Environmental Protection 129: 138-151

Mao Y, Schoeneich C, Asmus KD (1991): Identification of organic acids and other intermediates in oxidative degradation of chlorinated ethanes on titania surfaces en route to mineralization: a combined photocatalytic and radiation chemical study. The Journal of Physical Chemistry 95: 10080-10089

Martins JB, Andrés J, Longo E, Taft C (1996): H_2O and H_2 interaction with ZnO surfaces: a MNDO, AM1, and PM3 theoretical study with large cluster models. International journal of quantum chemistry 57: 861-870

Mattioli G, Filippone F, Caminiti R, Bonapasta AA (2008): Short hydrogen bonds at the water/TiO_2 (anatase) interface. The Journal of Physical Chemistry C 112: 13579-13586

Minero C, Maurino V, Vione D (2013): Photocatalytic mechanisms and reaction pathways drawn from kinetic and probe molecules. Photocatalysis and Water Purification: 53-72

Montoya JF, Ivanova I, Dillert R, Bahnemann DW, Salvador P, Peral J (2013): Catalytic role of surface oxygens in TiO_2 photooxidation reactions: Aqueous benzene photooxidation with $Ti_{18}O_2$ under anaerobic conditions. The Journal of Physical Chemistry Letters 4: 1415-1422

Montoya JF, Peral J, Salvador P (2014): Comprehensive kinetic and mechanistic analysis of TiO_2 photocatalytic reactions according to the direct–indirect model:(I) Theoretical approach. The Journal of Physical Chemistry C 118: 14266-14275

Mousavi SM, Mahjoub AR, Abazari R (2017): Facile green fabrication of nanostructural Ni-doped ZnO hollow sphere as an advanced photocatalytic material for dye degradation. J. Mol. Liq. 242: 512-519

Mrowetz M, Selli E (2006): Photocatalytic degradation of formic and benzoic acids and hydrogen peroxide evolution in TiO_2 and ZnO water suspensions. Journal of Photochemistry and Photobiology A: Chemistry 180: 15-22

Muhd Julkapli N, Bagheri S, Bee Abd Hamid S (2014): Recent advances in heterogeneous photocatalytic decolorization of synthetic dyes. The Scientific World Journal 2014

Munter R (2001): Advanced oxidation processes–current status and prospects. Proc. Estonian Acad. Sci. Chem 50: 59-80

Nagao M (1971): Physisorption of water on zinc oxide surface. The Journal of Physical Chemistry 75: 3822-3828

Navarro P, Gabaldón JA, Gómez-López VM (2017): Degradation of an azo dye by a fast and innovative pulsed light/H_2O_2 advanced oxidation process. Dyes and Pigments 136: 887-892

Norton P, Tapping R, Goodale J (1977): A photoemission study of the interaction of Ni (100),(110) and (111) surfaces with oxygen. Surface Science 65: 13-36

Nosaka Y, Yamashita Y, Fukuyama H (1997): Application of chemiluminescent probe to monitoring superoxide radicals and hydrogen peroxide in TiO_2 photocatalysis. The Journal of Physical Chemistry B 101: 5822-5827

Nosaka Y, Nosaka AY (2017): Generation and detection of reactive oxygen species in photocatalysis. Chem. Rev. 117: 11302-11336

Okamoto K-i, Yamamoto Y, Tanaka H, Tanaka M, Itaya A (1985): Heterogeneous photocatalytic decomposition of phenol over TiO_2 powder. Bull. Chem. Soc. Jpn. 58: 2015-2022

Patrick CE, Giustino F (2014): Structure of a water monolayer on the anatase TiO_2 (101) surface. Physical Review Applied 2: 014001

Peighambardoust NS, Asl SK, Mohammadpour R, Asl SK (2018): Band-gap narrowing and electrochemical properties in N-doped and reduced anodic TiO_2 nanotube arrays. Electrochim. Acta 270: 245-255

Pelizzetti E, Minero C (1993): Mechanism of the photo-oxidative degradation of organic pollutants over TiO_2 particles. Electrochim. Acta 38: 47-55

Peng J, Lu T, Ming H, Ding Z, Yu Z, Zhang J, Hou Y (2019): Enhanced Photocatalytic Ozonation of Phenol by Ag/ZnO Nanocomposites. Catalysts 9: 1006

Qian G, Peng Q, Zou D, Wang S, Yan B (2020): Hydrothermal Synthesis of Flake-Flower NiO and Its Gas Sensing Performance to CO. Frontiers in Materials 7: 216

Qian R, Zong H, Schneider J, Zhou G, Zhao T, Li Y, Yang J, Bahnemann DW, Pan JH (2019): Charge carrier trapping, recombination and transfer during TiO_2 photocatalysis: An overview. Catal. Today 335: 78-90

Rafiee M, Bashiri H (2019): Dynamic Monte Carlo simulations of the reaction mechanism of hydrogen production from formic acid on Ni(1 0 0). Appl. Surf. Sci. 475: 720-728

Rafiee M, Bashiri H (2020a): Catalytic decomposition of formic acid on Cu(100): Optimization and dynamic Monte Carlo simulation. Catal. Commun. 137: 105942

Rafiee M, Bashiri H (2020b): Application of response surface methodology and dynamic Monte Carlo simulation to study the hydrogen production from formic acid on Ni(100). Materials Science and Engineering: B 262: 114729

Rauf M, Meetani M, Hisaindee S (2011): An overview on the photocatalytic degradation of azo dyes in the presence of TiO_2 doped with selective transition metals. Desalination 276: 13-27

Reddy IN, Reddy CV, Sreedhar A, Shim J, Cho M, Yoo K, Kim D (2018): Structural, optical, and bifunctional applications: Supercapacitor and photoelectrochemical water splitting of Ni-doped ZnO nanostructures. J. Electroanal. Chem124-136 :828 .

Reina AC, Santos-Juanes L, Sánchez JG, López JC, Rubio MM, Puma GL, Pérez JS (2015): Modelling the photo-Fenton oxidation of the pharmaceutical paracetamol in water including the effect of photon absorption (VRPA). Applied Catalysis B: Environmental 166: 295-301

Rengifo-Herrera J, Pierzchała K, Sienkiewicz A, Forró L, Kiwi J, Pulgarin C (2009): Abatement of organics and Escherichia coli by N, S co-doped TiO_2 under UV and visible light. Implications of the formation of singlet oxygen ($^1O_2$) under visible light. Applied Catalysis B: Environmental 88: 398-406

Rothenberger G, Moser J, Graetzel M, Serpone N, Sharma DK (1985): Charge carrier trapping and recombination dynamics in small semiconductor particles. Journal of the American Chemical Society 107: 8054-8059

Ryu J, Choi W (2004): Effects of TiO_2 surface modifications on photocatalytic oxidation of arsenite: the role of superoxides. Environ. Sci. Technol. 38: 2928-2933

Sabouri Z, Akbari A, Hosseini HA, Darroudi M (2018): Facile green synthesis of NiO nanoparticles and investigation of dye degradation and cytotoxicity effects. J. Mol. Struct. 1173: 931-936

Safieddine D, Kachenoura A, Albera L, Birot G, Karfoul A, Pasnicu A, Biraben A, Wendling F, Senhadji L, Merlet I (2012): Removal of muscle artifact from EEG data: comparison between stochastic (ICA and CCA) and deterministic (EMD and wavelet-based) approaches. EURASIP Journal on Advances in Signal Processing 2012: 1-15

Sahel K, Elsellami L, Mirali I, Dappozze F, Bouhent M, Guillard C (2016 :(Hydrogen peroxide and photocatalysis. Applied Catalysis B: Environmental 188: 106-112

Salvador P (2007): On the nature of photogenerated radical species active in the oxidative degradation of dissolved pollutants with TiO_2 aqueous suspensions: a revision in the light of the electronic structure of adsorbed water. The Journal of Physical Chemistry C 111: 17038-17043

Samadi M, Ahmadi S, Poureshgh Y, Shabanloo A, Rahmani Z, Vanaei Tabar M (2017): Efficiency of Mn_2/H_2O_2 Process in Removal of ReactiveBlue 1 9Dyes from Aquatic Environments. Journal of Occupational and Environmental Health 2: 247-258

Sathishkumar P, Anandan S, Maruthamuthu P, Swaminathan T, Zhou M, Ashokkumar M (2011): Synthesis of Fe^{3+} doped TiO_2 photocatalysts for the visible assisted degradation of an azo dye. Colloids and Surfaces A: Physicochemical and Engineering Aspects 375: 231-236

Schneider J, Matsuoka M, Takeuchi M, Zhang J, Horiuchi Y, Anpo M, Bahnemann DW (2014): Understanding TiO_2 photocatalysis: mechanisms and materials. Chem. Rev. 114: 9919-9986

Sengunthar P, Bhavsar K, Balasubramanian C, Joshi U (2020): Physical properties and enhanced photocatalytic activity of ZnO-rGO nanocomposites. Appl. Phys. A 126: 1-9

Shampine LF, Reichelt MW (1997): The matlab ode suite. SIAM journal on scientific computing 18: 1-22

Shams Ghamsari Z, Bashiri H (2020): Hydrogen production through photoreforming of methanol by $Cu_{(s)}/TiO_2$ nanocatalyst: Optimization and simulation. Surfaces and Interfaces 21: 100709

Simion C, Florea O, Stanoiu A (2017): Gas sensing mechanism involved in H_2S detection with NiO loaded SnO_2 gas sensors. SCIENCE AND TECHNOLOGY 20: 415-425

Simon YDT, Hadis B, Estella TN, Arabamiri M, Serges D, Arnaud KT, Samuel L, Minoo T, Michael S, Reinhard S (2020): Urea and green tea like precursors for the preparation of g-C_3N_4 based carbon nanomaterials (CNMs) composites as photocatalysts for photodegradation of pollutants under UV light irradiation. Journal of Photochemistry and Photobiology A: Chemistry: 112596

Sivalingam G, Nagaveni K, Hegde M, Madras G (2003): Photocatalytic degradation of various dyes by combustion synthesized nano anatase TiO_2. Applied Catalysis B: Environmental 45: 23-38

Stets S, do Amaral B, Schneider JT, de Barros IR, de Liz MV, Ribeiro RR, Nagata N, Peralta-Zamora P (2018): Antituberculosis drugs degradation by UV-based advanced oxidation processes. Journal of Photochemistry and Photobiology A: Chemistry 353: 26-33

Tamaki Y, Furube A, Murai M, Hara K, Katoh R, Tachiya M (2007): Dynamics of efficient electron–hole separation in TiO_2 nanoparticles revealed by femtosecond transient absorption spectroscopy under the weak-excitation condition. Physical Chemistry Chemical Physics 9: 1453-1460

Tan S, Feng H, Ji Y, Wang Y, Zhao J, Zhao A, Wang B, Luo Y, Yang J, Hou J (2 :(012 Observation of photocatalytic dissociation of water on terminal Ti sites of TiO2 (110)-1× 1 surface. Journal of the American Chemical Society 134: 9978-9985

Tang X, Wang Z, Wang Y (2018): Visible active N-doped TiO_2/reduced graphene oxide for the degradation of tetracycline hydrochloride. Chem. Phys. Lett. 691: 408-414

Thiel PA, Madey TE (1987): The interaction of water with solid surfaces: Fundamental aspects. Surf. Sci. Rep. 7: 211-385

Turkten N, Cinar Z (2017): Photocatalytic decolorization of azo dyes on TiO_2: Prediction of mechanism via conceptual DFT. Catal. Today 287: 169-175

Vagı M, Petsas A (2017): Advanced oxidation processes for the removal of pesticides from wastewater: recent review and trends, 15th International Conference on Environmental Science and Technology. CEST2017, Rhodes, Greece

Verma AK, Dash RR, Bhunia P (2012): A review on chemical coagulation/flocculation technologies for removal of colour from textile wastewaters. Journal of Environmental Management 93: 154-168

Visan A, van Ommen JR, Kreutzer MT, Lammertink RG (2019): Photocatalytic Reactor Design: Guidelines for Kinetic Investigation. Industrial & Engineering Chemistry Research 58: 5349-5357

Vittadini A, Casarin M, Selloni A (2007): Chemistry of and on TiO_2-anatase surfaces by DFT calculations: a partial review. Theor. Chem. Acc. 117: 663-671

Wageh S, Almazroai LS, Alshahrie A, Al-Ghamdi AA (2018): Enhanced visible light photo-catalytic activity of ZnO and Ag-Doped ZnO (ZnO: Ag) nanoparticles. Journal of Nanoscience and Nanotechnology 18: 7682-7690

Wahab HS, Bredow T, Aliwi SM (2008): Computational investigation of water and oxygen adsorption on the anatase TiO_2 (1 0 0) surface. Journal of Molecular Structure: THEOCHEM 868: 101-108

Walle LE, Borg A, Johansson E, Plogmaker S, Rensmo H, Uvdal P, Sandell A (2011): Mixed dissociative and molecular water adsorption on anatase TiO_2 (101). The Journal of Physical Chemistry C 115: 9545-9550

Wan X, Ma R, Tie S, Lan S (2014): Effects of calcination temperatures and additives on the photodegradation of methylene blue by tin dioxide nanocrystals. Mater. Sci. Semicond. Process. 27: 748-757

Wang X-q, Han S-f, Zhang Q-w, Zhang N, Zhao D-d (2018): Photocatalytic oxidation degradation mechanism study of methylene blue dye waste water with GR/TiO_2, MATEC Web of Conferences. EDP Sciences, pp. 03006

Wang Y, Shi R, Lin J, Zhu Y (2010): Significant photocatalytic enhancement in methylene blue degradation of TiO_2 photocatalysts via graphene-like carbon in situ hybridization. Applied Catalysis B: Environmental 100: 179-183

Westall F, Brack A (2018): The importance of water for life. Space Science Reviews 214: 50

Wu X, Selloni A, Lazzeri M, Nayak SK (2003): Oxygen vacancy mediated adsorption and reactions of molecular oxygen on the TiO_2 (110) surface. Physical Review B 68: 241402

Xia Y, Wang J, Chen R, Zhou D, Xiang L (2016): A review on the fabrication of hierarchical ZnO nanostructures for photocatalysis application. Crystals 6: 148

Yao S, Qu F, Wang G, Wu X (2017): Facile hydrothermal synthesis of WO_3 nanorods for photocatalysts and supercapacitors. J. Alloys Compd. 724: 695-702

Yoneyama H, Torimoto T (2000): Titanium dioxide/adsorbent hybrid photocatalysts for photodestruction of organic substances of dilute concentrations. Catal. Today 58: 133-140

Yu JC, Lin J, Lo D, Lam S (2000): Influence of thermal treatment on the adsorption of oxygen and photocatalytic activity of TiO_2. Langmuir 16: 7304-7308

Yu L, Wang L, Sun X, Ye D (2018): Enhanced photocatalytic activity of rGO/TiO_2 for the decomposition of formaldehyde under visible light irradiation. Journal of Environmental Sciences 73: 138-146

Yue X, Zhang T, Yang D, Qiu F, Fang J (2018): In situ fabrication dynamic carbon fabrics membrane with tunable wettability for selective oil–water separation. Journal of Industrial and Engineering Chemistry 61: 188-196

Zheng Q, Ross J (1991): Comparison of deterministic and stochastic kinetics for nonlinear systems. The Journal of Chemical Physics 94: 3644-3648

Zhou Z, Liu X, Sun K, Lin C, Ma J, He M, Ouyang W (2019): Persulfate-based advanced oxidation processes (AOPs) for organic-contaminated soil remediation: A review. Chem. Eng. J. 372: 836-851

1326

1327

Tables:

Table 1. The systems used to assess the feasibility of applying the proposed approach to predict the photodegradation of the organic pollutants.

The studied system	[photocatalyst]	[pollutant]	[The other materials]	pH	Ref.
Acid Orange 7/Fe-doped TiO_2/ UV-light	100 $mg.L^{-1}$	50 $mg.L^{-1}$	3 wt. %	3-9	(Han et al. 2018)
Congo Red /Ni-doped ZnO/ UV-light	0.5 $g.L^{-1}$	10 $mg.L^{-1}$	Ni-to-Zn weight ratios (2%, 3%, 5%, and 10%)	6	(Mousavi et al. 2017)
Tetracycline hydrochloride /N-doped TiO_2 and N-doped TiO_2/RGO/visible light	1 $g.L^{-1}$	10 $mg.L^{-1}$	-	neutral	(Tang et al. 2018)
Phenol/ZnO/O_3, Ag-doped ZnO and Ag-doped ZnO/O_3/ UV-light	0.5 $g.L^{-1}$	50 $mg.L^{-1}$	$[O_3(gas)]$=10 $mg.L^{-1}$ [Ag]=1.5 wt. %	6.8	(Peng et al. 2019)

Table 2. Proposed formulations of the reactive-centers on the photocatalyst surface in contact with the pollutant aqueous solution.

The type of reactive-center	Formula
RC1	$M-OH$, $M-OH_2^+$, $M-O^-$, $M-OH_2$, $M-O_{bridge}H-M$, and $M-O_{bridge}(H_2O)-M$
RC2	$A-OH$, $A-OH_2^+$, $A-O^-$, $A-OH_2$, $A-O_{bridge}H-X$, and $A-O_{bridge}(H_2O)-X$
RC3	$M-O_2$ ($Ti-O_2$ or $Zn-O_2$)
RC4	$A-O_2$ ($Fe-O_2 or\ Ag-O_2 or\ Ni-O_2$)
RC5	$B-O_2$ ($rGO-O_2$)
RC6	Species adsorbed (C) on the surface of the photocatalyst (such as O_3)
RC7	The effective reactive-centers such as $Ti^{4+}$and Zn^{2+} for the trapping of photogenerated electrons
RC8	The effective reactive-centers such as $>O^{2-}$and OH^- for the trapping of photogenerated holes
RC9	The other effective reactive-centers (A^{m+}) such as Fe^{3+} , Ni^{2+} and Ag^+ for the trapping of photogenerated electrons
RC10	$S_{inactive}$ (for hydroxyl radicals)
RC11	$S_{inactive}$ (for superoxide radicals)
RC12	$S_{inactive}$ (for other species)
RC13	Adsorption sites

Table 3. The general proposed framework for the mechanism of the degradation process of the organic pollutants in $\{A-\text{doped } M_xO_y/B/UV-Vis\}$ aqueous systems.

Part 1: The generation of charge carriers:

$A-\text{doped } M_xO_y/B + I_{\text{eff}} \rightarrow h^+ + e^-$

Part 2: Adsorption of the organic pollutant on the photocatalyst surface:

$RC7 + \text{pollutant} \leftrightarrows \text{pollutant(ads)}$

Part 3: The trapping of the charge carriers:

$RC1 + h^+ \rightarrow OH^\bullet(ads)$

$RC2 + h^+ \rightarrow OH^\bullet(ads)$

$RC8 + h^+ \rightarrow h^+_{\text{trapped}}$

$\text{Pollutant(ads)} + h^+ \rightarrow \text{Intermediates}$

$RC3 + e^- \rightarrow O_2^{-\bullet}(ads)$

$RC4 + e^- \rightarrow O_2^{-\bullet}(ads)$

$RC5 + e^- \rightarrow O_2^{-\bullet}(ads)$

$RC6 + e^- \rightarrow O_2^{-\bullet}(ads)$

$RC7 + e^- \rightarrow e^-_{\text{trapped}}$

$RC9 + e^- \rightarrow O_2^{-\bullet}(ads)$

$O_2^{-\bullet}(ads) + 2H^+ + e^- \rightarrow H_2O_2(ads)$

$H_2O_2(ads) + e^- \rightarrow OH^\bullet(ads) + OH^-$

Part 4: The reaction of ROSs with the organic pollutant molecules

$OH^\bullet(ads) + \text{pollutant} \rightarrow \text{Intermediates}$

$O_2^{-\bullet}(ads) + \text{pollutant} \rightarrow \text{Intermediates}$

Part 5: The reaction of ROSs with the intermediates:

$\text{Intermediates} + OH^\bullet(ads) \rightarrow \text{products}$

$\text{Intermediates} + O_2^{-\bullet}(ads) \rightarrow \text{products}$

Part 6: The recombination of the e^-/h^+ pairs:

$h^+_{\text{trapped}} + e^-_{\text{trapped}} \rightarrow \text{heat}$

$h^+ + e^- \rightarrow \text{heat}$

Part 7: The inactivation of the ROSs by the inactive species:

$RC10 + OH^\bullet(ads) \rightarrow \text{Inactivated species}$

$RC11 + O_2^{-\bullet}(ads) \rightarrow \text{Inactivated species}$

$RC12 + \text{The other radicals} \rightarrow \text{Inactivated species}$

Table 4. The elementary reaction steps and their rate constants (the fitted results and the reported values in the literature) for the mechanism of the degradation process of the organic pollutants in the studied systems.

I.D.	Elementary reactions	The fitted rate constants (k) (Adjusted-optimized)				
		Fe-doped TiO_2	Ni-doped ZnO	N-doped TiO_2	N-doped TiO_2/RGO	Ag-doped ZnO/O_3
1	$A-doped\ M_xO_y/B/C + I_{eff} \rightarrow e^- + h^+$	1.49×10^{-3} (M^{-1} . min^{-1})	1.032×10^{-3} (M^{-1} . min^{-1})	1.18×10^{-1} (M^{-1} . min^{-1})	1.78×10^{-1} (M^{-1} . min^{-1})	1.71×10^{-3} (M^{-1} . min^{-1})

2	$h^+ + M - OH \rightarrow OH^{\bullet}_{ads}$	6.30×10^{9} (M^{-1} . min^{-1})	8.39×10^{9} (M^{-1} . min^{-1})	-	-	8.30×10^{9} (M^{-1} . min^{-1})
3	$h^+ + pollutant_{ads} \rightarrow 2intermediate1$	1.00×10^{9} (M^{-1} . min^{-1})	1.00×10^{9} (M^{-1} . min^{-1})	9.53×10^{7} (M^{-1} . min^{-1})	9.53×10^{7} (M^{-1} . min^{-1})	2.10×10^{9} (M^{-1} . min^{-1})
4	$h^+ + A - OH \rightarrow OH^{\bullet}_{ads}$	6.30×10^{9} (M^{-1} . min^{-1})	8.30×10^{9} (M^{-1} . min^{-1})	-	-	7.30×10^{9} (M^{-1} . min^{-1})
5	$h^+ + S_{trapping2} \rightarrow h_{trapped}$	3.92×10^{9} (M^{-1} . min^{-1})	3.92×10^{9} (M^{-1} . min^{-1})	1.49×10^{9} (M^{-1} . min^{-1})	1.49×10^{9} (M^{-1} . min^{-1})	1.89×10^{9} (M^{-1} . min^{-1})
6	$e^- + A \rightarrow A^-$	1.73×10^{9} (M^{-1} . min^{-1})	-	-	-	7.86×10^{9} (M^{-1} . min^{-1})
7	$M - O_2 + e^- \rightarrow O^{\bullet-}_{2ads}$	6.20×10^{9} (M^{-1} . min^{-1})	6.20×10^{9} (M^{-1} . min^{-1})	5.49×10^{9} (M^{-1} . min^{-1})	5.49×10^{9} (M^{-1} . min^{-1})	7.70×10^{9} (M^{-1} . min^{-1})
8	$A - O_2 + e^- \rightarrow O^{\bullet-}_{2ads}$	7.30×10^{9} (M^{-1} . min^{-1})	7.30×10^{9} (M^{-1} . min^{-1})	-	-	-
9	$e^- + M - C \rightarrow C^{\bullet-}(O^{\bullet-}_3(ads))$	-	-	-	-	9.00×10^{9} (M^{-1} . min^{-1})
10	$e^- + S_{trapping1} \rightarrow e_{trapped}$	4.89×10^{9} (M^{-1} . min^{-1})	4.82×10^{9} (M^{-1} . min^{-1})	5.49×10^{9} (M^{-1} . min^{-1})	4.49×10^{9} (M^{-1} . min^{-1})	3.02×10^{9} (M^{-1} . min^{-1})
11	$e^- + B - O_2 \rightarrow O^{\bullet-}_{2ads}$	-	-	-	6.53×10^{7} (M^{-1} . min^{-1})	-
12	$O^{\bullet-}_{2ads} + 2H^+ + e^- \rightarrow H_2O_{2ads}$	1.42×10^{12} (M^{-1} . min^{-1})	1.42×10^{12} (M^{-1} . min^{-1})	9.53×10^{11} (M^{-1} . min^{-1})	9.53×10^{11} (M^{-1} . min^{-1})	2.30×10^{11} (M^{-1} . min^{-1})
13	$H_2O_{2ads} + e^- \rightarrow OH^{\bullet}_{ads} + OH^-$	2.59×10^{9} (M^{-1} . min^{-1})	2.59×10^{9} (M^{-1} . min^{-1})	2.53×10^{9} (M^{-1} . min^{-1})	2.53×10^{9} (M^{-1} . min^{-1})	2.80×10^{9} (M^{-1} . min^{-1})
14	$A^- + M - O_2 \rightarrow O^{\bullet-}_{2ads}$	9.20×10^{8} (M^{-1} . min^{-1})	-	-	-	9.20×10^{8} (M^{-1} . min^{-1})
15	$A^- + M - O_3 \rightarrow O^{\bullet-}_3(ads)$	-	-	-	-	9.50×10^{8} (M^{-1} . min^{-1})
16	$O^{\bullet-}_3(ads) + H^+ \rightarrow HO^{\bullet-}_3(ads)$	-	-	-	-	3.23×10^{10} (M^{-1} . min^{-1})
17	$HO^{\bullet-}_3(ads) \rightarrow O^{\bullet-}_3(ads) + H^+$	-	-	-	-	3.45×10^{5} (M^{-1} . min^{-1})
18	$HO^{\bullet-}_3(ads) \rightarrow OH^{\bullet}_{ads} + O_2$		-	-	-	3.20×10^{5} (M^{-1} . min^{-1})
19	$O^{\bullet-}_{2ads} + M - O_3 \rightarrow O^{\bullet-}_3(ads)$	-	-	-	-	6.00×10^{9} (M^{-1} . min^{-1})
20	$pollutant + Site \rightarrow pollutant_{ads}$	4×10^{1} (M^{-1} . min^{-1})	2.1×10^{2} (M^{-1} . min^{-1})	7.92×10^{2} (M^{-1} . min^{-1})	1.20×10^{3} (M^{-1} . min^{-1})	2.75×10^{2} (M^{-1} . min^{-1})
21	$pollutant_{ads} \rightarrow pollutant + Site$	1×10^{-3} (min^{-1})	1.59×10^{2} (min^{-1})	7.50×10^{2} (min^{-1})	8.5×10^{1} (min^{-1})	2.12×10^{2} (min^{-1})
22	$pollutant + OH^{\bullet}_{ads} \rightarrow 2intermediate2$	9.20×10^{6} (M^{-1} . min^{-1})	5.02×10^{7} (M^{-1} . min^{-1})	9.53×10^{7} (M^{-1} . min^{-1})	9.53×10^{7} (M^{-1} . min^{-1})	8.70×10^{7} (M^{-1} . min^{-1})
23	$pollutant + O^{\bullet-}_{2ads} \rightarrow 2intermediate3$	5.03×10^{3} (M^{-1} . min^{-1})	8.30×10^{4} (M^{-1} . min^{-1})	9.53×10^{3} (M^{-1} . min^{-1})	3.79×10^{3} (M^{-1} . min^{-1})	7.30×10^{3} (M^{-1} . min^{-1})
24	$pollutant + M - C \rightarrow 2intermediate4$	-	-	-	-	2.52×10^{2} (M^{-1} . min^{-1})
25	$intermediate2 + OH^{\bullet}_{ads} \rightarrow Products$	5.18×10^{6} (M^{-1} . min^{-1})	6.90×10^{6} (M^{-1} . min^{-1})	-	-	6.68×10^{6} (M^{-1} . min^{-1})

26	$intermediate3+O_{2ads}^{\bullet-} \rightarrow Products$	6.03×10^{3} (M^{-1} . min^{-1})	5.38×10^{4} (M^{-1} . min^{-1})	9.79×10^{3} (M^{-1} . min^{-1})	2.11×10^{3} (M^{-1} . min^{-1})	1.60×10^{3} (M^{-1} . min^{-1})
27	$e_{trapped} + h_{trapped} \rightarrow heat$	3.56×10^{9} (M^{-1} . min^{-1})	7.86×10^{9} (M^{-1} . min^{-1})	-	-	3.92×10^{8} (M^{-1} . min^{-1})
28	$e^{-} + h^{+} \rightarrow heat$	4.59×10^{9} (M^{-1} . min^{-1})	8.90×10^{9} (M^{-1} . min^{-1})	6.48×10^{8} (M^{-1} . min^{-1})	6.45×10^{8} (M^{-1} . min^{-1})	8.30×10^{9} (M^{-1} . min^{-1})
29	$S1_{inactive} + OH_{ads}^{\bullet} \rightarrow inactive$	8.00×10^{6} (M^{-1} . min^{-1})	8.00×10^{6} (M^{-1} . min^{-1})	-	-	1.10×10^{7} (M^{-1} . min^{-1})
30	$S2_{inactive} + O_2^{-\bullet}$(ads) → Inactivated species	-	-	1.53×10^{3} (M^{-1} . min^{-1})	1.53×10^{3} (M^{-1} . min^{-1})	6.50×10^{3} (M^{-1} . min^{-1})
31	$S3_{inactive}$(ads) $+ M - C$ → Inactivated species	-	-	-	-	1.25×10^{2} (M^{-1} . min^{-1})

1341

Table 5. The elementary reaction steps and their rate constants (the fitted results and the reported values in the literature) for the mechanism of the TC degradation in the TiO_2/visible light. 1342 1343

I.D.	Elementary reactions	The adjusted rate constants (M^{-1}.min^{-1})	The optimized rate constants (M^{-1}.min^{-1})
1	Site + TC → TC(ads)	1.12×10^{2}	1.13×10^{2}
2	TC(ads) → Site + TC	6.30×10^{1}	6.46×10^{1}
3	TC(ads) + I_{eff} → TC(ads)* + e^{-}	2.70×10^{-4}	1.56×10^{-4}
4	$O_2^{-\bullet} + e^{-} \rightarrow O_2^{-\bullet}$(ads)	5.49×10^{8}	5.49×10^{8}
5	$O_2^{-\bullet}$(ads) + TC → Intermediates	6.79×10^{3}	6.79×10^{3}
6	Intermediates + $O_2^{-\bullet}$(ads) → products	1.53×10^{4}	1.53×10^{4}
7	TC(ads)* + e^{-} → heat	6.48×10^{7}	6.48×10^{7}
8	$S_{inactive} + O_2^{-\bullet}$(ads) → Inactivated species	1.63×10^{3}	1.63×10^{3}

1344

Figures:

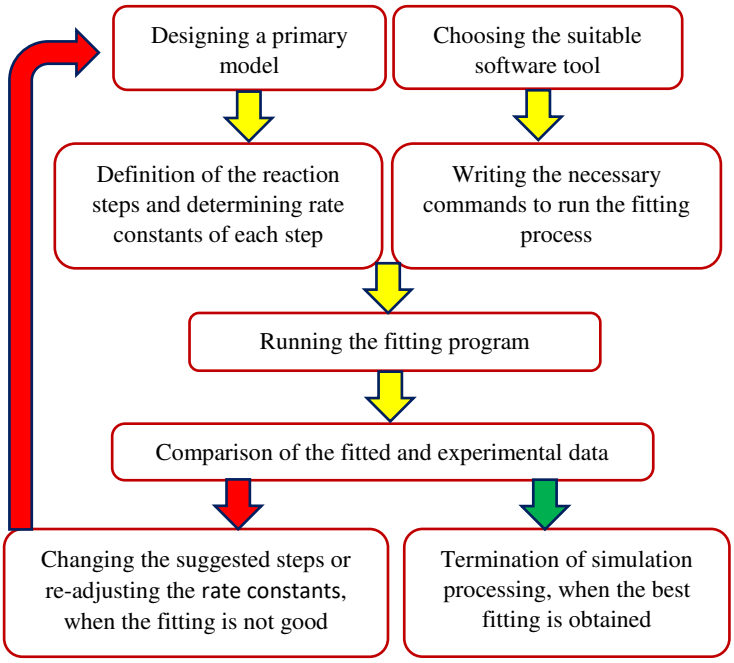

Figure 1. An overview of the proposed approach.

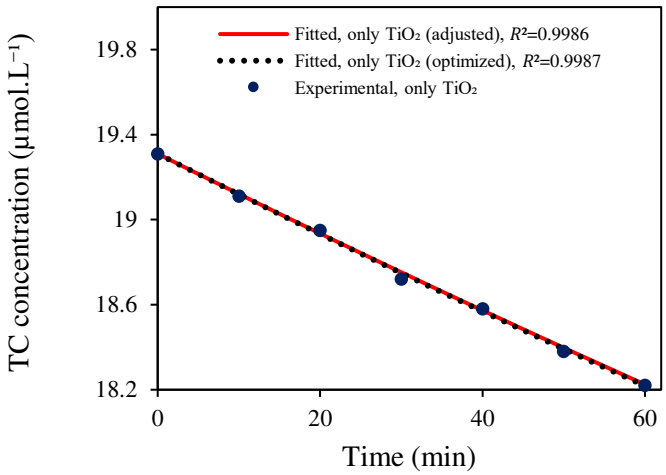

Figure 2. Implementing the proposed approach to find the best mechanism of the TC degradation in the TiO_2/visible-light system by comparing the two optimization and manual adjustment methods.

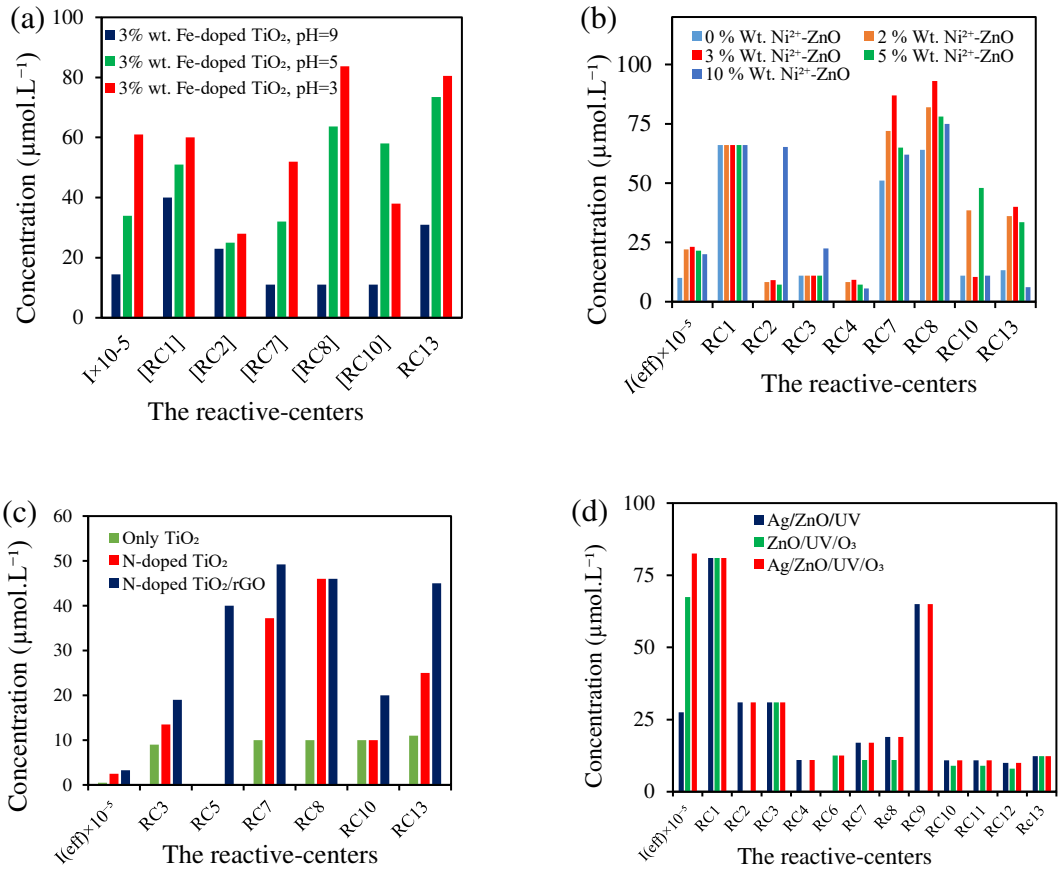

Figure 3. The effective concentration of the reactive-centers obtained from implementing the fitting process for all the studied samples.

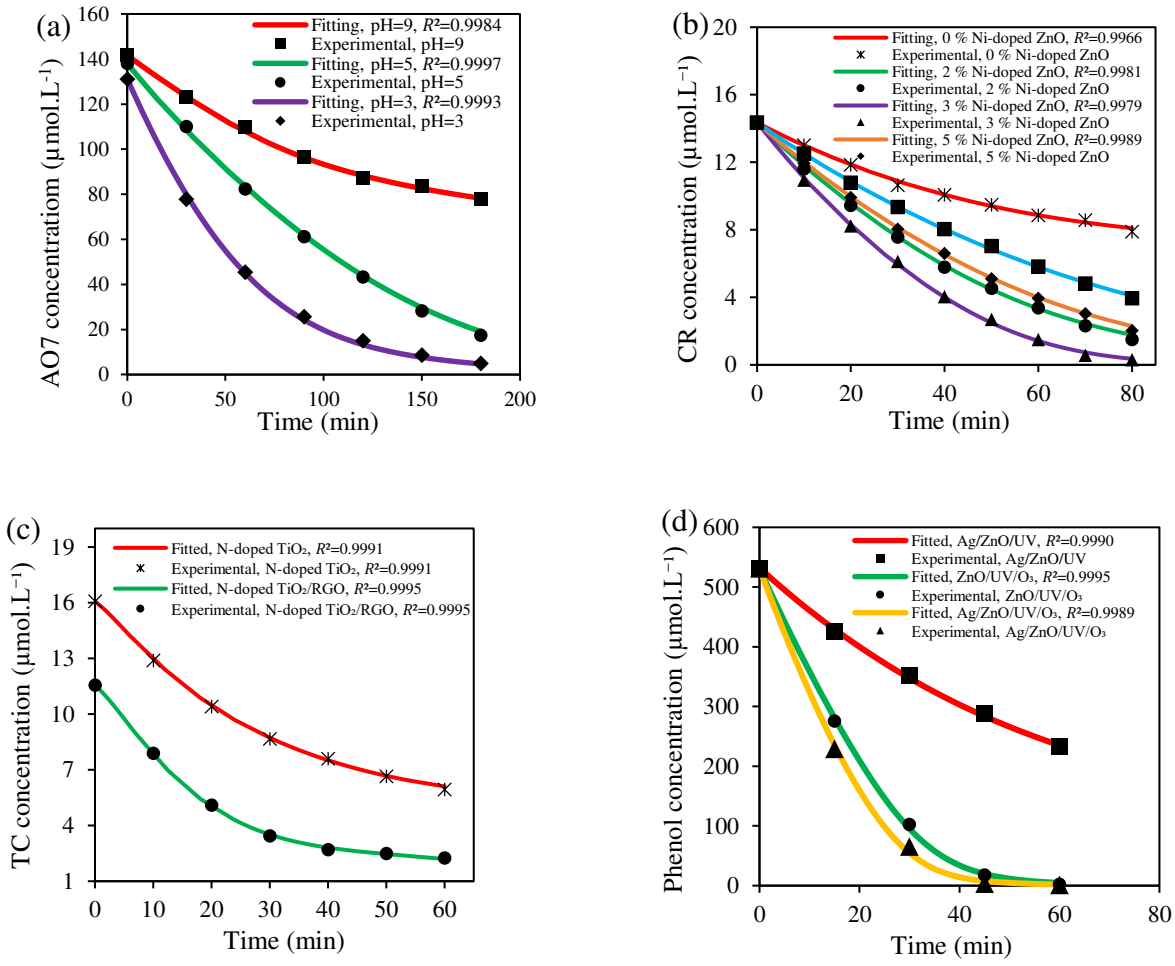

Figure 4. The curves of the organic pollutant concentration vs. time for the studied systems (the experimental and the fitted results).

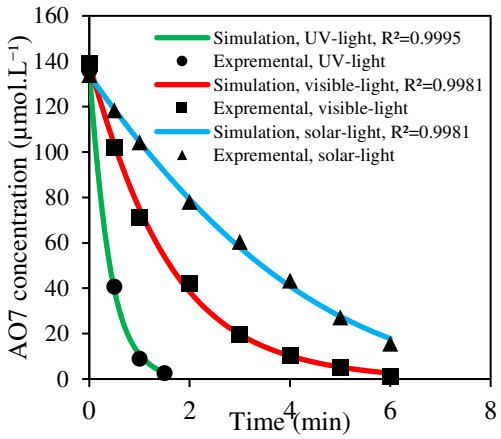

Figure 5. Comparison of the AO7 photodegradation on the 2wt.% Fe-doped TiO_2 surface induced by different light sources (the experimental and the fitted results).